The University of South Bohemia in České Budějovice
Faculty of Science

Encapsulation of bacterial photosynthetic reaction centers into viral capsids

Bachelor's Thesis

Author
Guy Wolf

Supervisor
Mgr. David Kaftan, PhD.

Co-Supervisor
prof. Mgr. Roman Tuma, PhD.

České Budějovice, 2023

Wolf G., 2023: Encapsulation of bacterial photosynthetic reaction centers into viral capsids. Bc. Thesis, in English 42 p., Faculty of Science, University of South Bohemia, České Budějovice, Czech Republic.

Annotation:

The final aim of this thesis was to achieve the encapsulation of photosynthetic reaction centers with light harvesting complex 1 from *Rhodobacter sphaeroides* into viral capsids of bacteriophage P22. To this end, the reaction centers and the capsids had to be isolated and purified first. The capsids are composed of a coat protein forming the stable outer shell and a scaffolding protein driving the self-assembly of the capsids and forming its inner lining. Therefore, scaffolding proteins could be used to introduce the reaction center into the capsids. To achieve that, the scaffolding protein was successfully functionalized with an NTA-maleimide linker for binding with the HisTag of the reaction center's H subunit, creating a reaction center-scaffolding protein complex. By inducing self-assembly of the capsid's components with this complex, the reaction centers were successfully encapsulated. This was confirmed by transmission electron microscopy pictures showing the encapsulated reaction centers. These engineered virus-like particles containing photosystems are therefore a first step towards the assembly of a nanoreactor featuring a photosynthetic reaction center powering a cascade of chemical reactions performed by additionally co-encapsulated enzymes.

Declaration:

I declare that I am the author of this qualification thesis and that in writing it I have used the sources and literature displayed in the list of used sources only.

Linz, 11th of May 2023.

Guy Wolf

Acknowledgements:

I would like to express my sincere gratitude to my supervisor, Mgr. David Kaftan, Ph.D., for his constant support and dedication. He always made time to help me with my work, explaining concepts and being available whenever I had questions.

I want to acknowledge prof. Mgr. Roman Tůma, Ph.D. without whom this project wouldn't exist and who helped a lot especially during the finalization of the work.

I am also grateful to Paulina Duhita Anindita, Ph.D, for her assistance especially with the molecular biology aspects of the practical work. It helped me very much and I could learn a lot.

Additionally, I would like to thank the rest of the team for their support and help during the daily lab work, making it really enjoyable to visit the lab.

Thank you all!

Table of Contents

1. Introduction

1.1. Photosynthesis

Photosynthesis is a fundamental bioenergetic process that occurs in a diverse range of organisms, including plants, algae, and some bacteria. It is the process by which light energy is converted into chemical energy that can be used by cells to fuel metabolic reactions. The process involves the capture of light energy by pigments, such as chlorophyll and carotenoids, which are located in specialized organelles called chloroplasts in plants and algae, and in specialized membranes called chromatophores in some bacteria, like *Rhodobacter (R.) sphaeroides* (Blankenship, 2014; Nelson & Yocum, 2006; Taiz & Zeiger, 2010).

Photosynthesis can be divided into two main stages: the light-dependent reactions and the light-independent reactions. During the light-dependent reactions, light energy is absorbed by the pigments and is used to generate transmembrane electrochemical potential (subsequently harnessed for ATP synthesis) and to reduce electron carriers in the electron transport chain reducing NADP+ to NADPH. These energy-rich molecules are then used in the light-independent reactions, also known as the Benson-Bassham-Calvin cycle, to synthesize organic compounds from carbon dioxide and water - primarily sugars and subsequently also amino and nucleic acids, fatty acids etc. (Nelson & Yocum, 2006; Taiz & Zeiger, 2010).

The process of photosynthesis has significant implications for the global ecosystem and for human society. For example, photosynthesis is responsible for producing the majority of the oxygen in Earth's atmosphere, making it essential for the survival of most organisms. Additionally, photosynthesis plays a critical role in the global carbon cycle, in which carbon dioxide is taken up by plants and marine phytoplankton during photosynthesis and is then released again during cellular respiration or combustion. (Blankenship, 2014; Eaton-Rye et al., 2012)

Moreover, photosynthesis has important implications for agriculture and human nutrition. By producing organic compounds, such as carbohydrates and proteins, photosynthesis provides the basis for most food webs on Earth. Additionally, the study of photosynthesis has led to the development of technologies, such as solar panels and biofuels, that transform the energy of the sun into forms usable by humans. (Blankenship, 2014; Eaton-Rye et al., 2012)

In total, it can be said that photosynthesis is a complex and vital process that occurs in a diverse range of organisms. Its study has led to significant advances in our understanding of the natural world and has practical implications for human society.

1.1.1. Photosynthetic reactions

There are two major types of photosynthesis called oxygenic and anoxygenic. As the names suggest, oxygenic photosynthesis involves the oxidation of water to oxygen, while anoxygenic photosynthesis primarily involves the creation of an electrochemical potential across the membrane without net reduction or oxidation of substrates (Blankenship, 2014).

Oxygenic photosynthesis is the most well-known form of photosynthesis and is found in cyanobacteria, algae, and plants. This process involves two photosystems, photosystem I (PSI) and photosystem II (PSII), working together by capturing light to generate ATP and NADPH while producing oxygen as a byproduct. PSII oxidizes water to release electrons, which are transferred to PSI via the electron transport chain, reducing NADP+ to NADPH. Parallel to the electron transfer, proton motive force across the thylakoid membrane is generated that powers photophosphorylation generating ATP. The schematic pathway can be observed in **Figure 1** (Blankenship, 2014; Nelson & Ben-Shem, 2004).

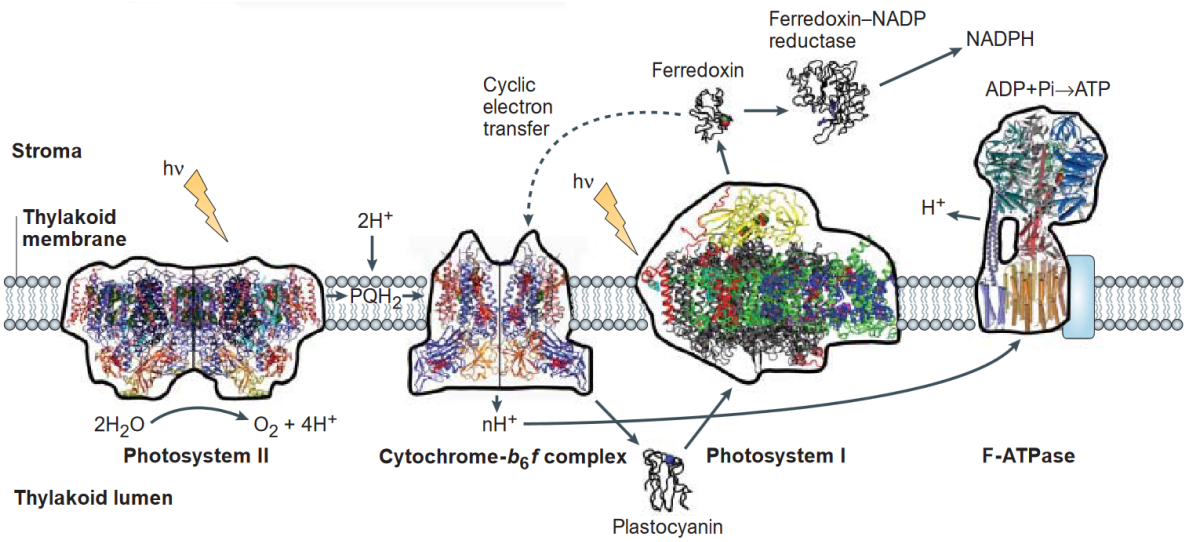

Figure 1 schematic depiction of the four large membrane-protein complexes driving oxygenic photosynthesis embedded in the thylakoid membranes (Nelson & Ben-Shem, 2004)

Anoxygenic photosynthesis, of interest for our study, emerged before the oxygenic photosynthesis and evolved over a very long time span. It is however considered by some ecologists not as important as oxygenic photosynthesis because of its lacking capacity to

produce oxygen and its comparable impact on the environment seems to be less significant. The anoxygenic phototrophs utilize only one of the two types of photosystems, depending on the organism, and use different types of bacteriochlorophylls as photo-pigment instead of chlorophyll, therefore absorbing light at different wavelengths, generally extending their light harvesting into the infra-red region (Hanada, 2016).

As can be seen in **Figure 2** the reaction center (RC) is surrounded by so called light-harvesting (LH) complexes capturing the energy of the light and channeling it to the RC. There, the special pair of bacteriochlorophylls gets excited and donates electrons over an electron transport chain to the quinone pool. By accepting the electrons, the quinone takes up two protons from the cytoplasm and migrates through the membrane to transfer its electrons to the cytochrome c_2 over cytochrome bc_1. Thereby, the protons are released into the periplasm creating a transmembrane electrochemical gradient. ATP can then be generated by the ATP-synthase using that gradient, storing the captured energy. To close the electron transfer cycle, the cytochrome c_2 migrates to the RC reducing the primary electrons donors (Adessi & De Philippis, 2013; Blankenship, 2014; Madigan et al., 2010).

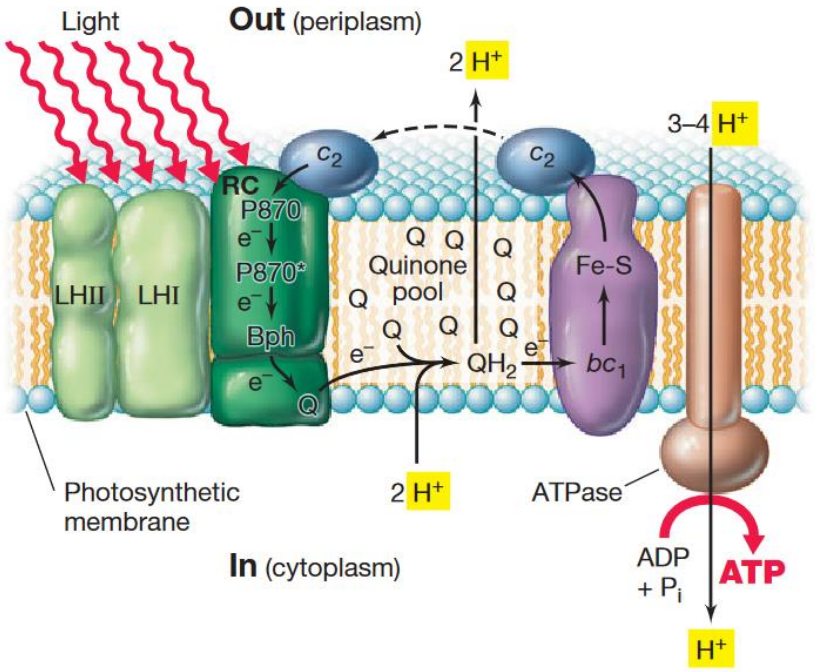

Figure 2 schematic visualization of the protein complexes involved in anoxygenic photosynthesis of purple bacetria embedded in the chromatophores including electron and proton transport (Madigan et al., 2010)

1.1.2. Photosynthesis for future technologies

Since photosynthesis is one of the fundamental processes driving life on earth as mentioned above, we humans tried to mimic and improve its principle for industrial use to serve our increasing energy needs. Especially today, renewable energy sources need to be exploited in order to replace fossil fuels and reduce CO_2 emissions. Therefore, the use of photosynthesis seems to be one of the best solutions, by being able to replace fossil fuels and capturing CO_2 from the atmosphere thereby decreasing its concentration.

To achieve that, several concepts were developed in the past such as simply converting biomass into biofuels (Potters et al., 2010) or using biophotovoltaics based on the coupling of the photosynthetic reaction centers with electrodes (Ciornii et al., 2017; Friebe & Frese, 2017). The last-mentioned reaction centers were already successfully introduced into liposomes along with quantum dots having higher light-capturing efficiencies than the natural light-harvesting proteins thereby potentially increasing the yield and durability of the hybrid systems (Lukashev et al., 2016). It was even possible to improve natural photosynthesis by coupling reaction centers and enzymes in a synthetic way to achieve a higher efficiency than nature (Lubner et al., 2011).

All these advancements suggest that the use of photosynthetic organisms and especially their photosynthetic reaction centers might be of use for future green technologies.

1.2. *Rhodobacter sphaeroides*

R. sphaeroides is a purple non-sulphur bacterium capable of photosynthesis that is found in freshwater habitats preferring anoxic environment such as lake sediments. Its genome consists of 2 chromosomes and mostly 5 plasmids (Aizawa, 2014). It is a very versatile bacterium that is able to perform anoxygenic photosynthesis, fermentation and aerobic or anaerobic respiration. Therefore, the type of metabolism depends mostly on the oxygen concentration (Mackenzie et al., 2007). With these features it is a perfect candidate for the biotechnological industry being able to utilize different starting materials and growing under different conditions. It is, however, not implemented yet to its full potential. (Orsi et al., 2021)

In general, it is a well-studied organism often used in research. Especially in biological photosynthesis it is considered a model organism for the expression of photosynthetic proteins, dealt with in the next part (Jaschke et al., 2011).

1.2.1. Photosystem of *Rhodobacter sphaeroides*

The photosystem of *R. sphaeroides* is well studied and therefore of interest for following research dealing with photosynthesis and reaction centers (Lukashev et al., 2016; Ravi et al., 2019). As can be seen in **Figure 3** the core of the photosystem consists of a dimer of photosynthetic reaction centers together with the PufX protein and protein-U surrounded by the S-shaped light-harvesting 1 (LH1) complex. RC-LH1 is also present as monomer, where only one RC is surrounded by a C-shaped LH1. In both, PufX protein plays a role in electron transfer and protein-U seems to have an influence on the dimer formation and stabilization. α/β heterodimer subunits on the other hand form the LH1 complex and bind bacteriochlorophyll and carotenoid pigments for light absorption. (Jaschke et al., 2011; Tani et al., 2022)

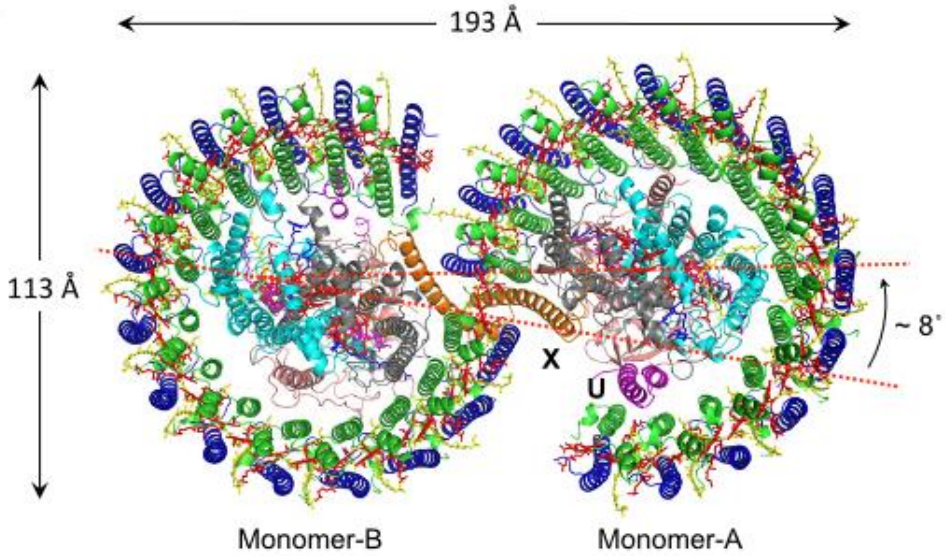

Figure 3 scheme of the RC-LH1 complex of *Rhodobacter sphaeroides* embedded in the cytoplasmic membrane consisting of the reaction centers (RC), the light-harvesting 1 (LH1) complex, the PufX protein (orange) and protein-U (magenta). (Tani et al., 2022)

Besides the robustness of the *R. sphaeroides* RC, which makes it a great tool for studying photosynthesis and using it for other purposes like bio-photovoltaics (Yaghoubi et al., 2012), great advancements have also been made in the efficiency of its purification (Jun et al., 2014). These advancements might make the RC of *R. sphaeroides* a good candidate for industrial applications.

As can be observed in **Figure 4** the reaction center itself consists of three protein subunits named L, M and H. The H subunit anchored by its single transmembrane helix is situated on the cytoplasmic side of the membrane, whereas the L and M subunit can be observed to be

integral membrane proteins. Together they built the support for the 10 cofactors forming the electron transport chain responsible for the charge separation in the RC. This transport chain starts with the special pair (P) composed of a dimer of specifically arranged bacteriochlorophylls a (BChl a) absorbing photons leading to an electron-exited state transferred to another BChl (B_A), a bacteriopheophytin (BPhe; H_A) and two ubiquinones (Q_A and Q_B) in a series of redox reactions. There is also another BChl (B_B) with a second BPhe (H_B), a non-heme iron and a carotenoid. Considering all its characteristics and a quantum efficiency of close to 1 for the charge separation, this RC seems to be a good choice for energy capturing applications. (Blankenship, 2014; Jun et al., 2018)

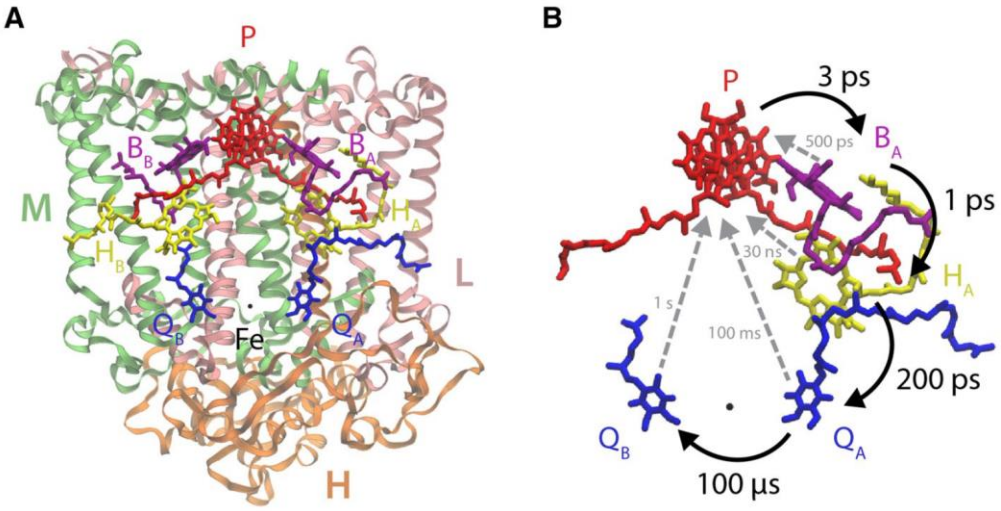

Figure 4 model of reaction center and cofactors **A** reaction center with L (pink), M (green) and H (orange) subunits containing the following cofactors: special pair P (red); BChls B_A and B_B (purple); BPhes H_A and H_B (yellow); quinones Q_A and Q_B (blue); non-heme iron (black) and carotenoid (not shown) **B** cofactors involved in charge separation with forward electron transfer time constants (black arrows) and reverse recombination time constants to ground state (grey arrows). (Jun et al., 2018)

1.3. P22 virus like particles

1.3.1. Bacteriophage P22

Bacteriophage P22 is a temperate double-stranded DNA phage of *Salmonella thyphimurium* and a relative of bacteriophage λ with which it shares many similarities. The structure and biology of P22 is very well studied and is therefore ideal to build synthetic constructs on its basis (O'Neil et al., 2011). Usually, assembly of a full infectious virion consists of two separated pathways, namely the assembly of the capsid and of the tail, that later fuse to form the virion. The focus in this case lies on the capsid. (Calendar, 2005)

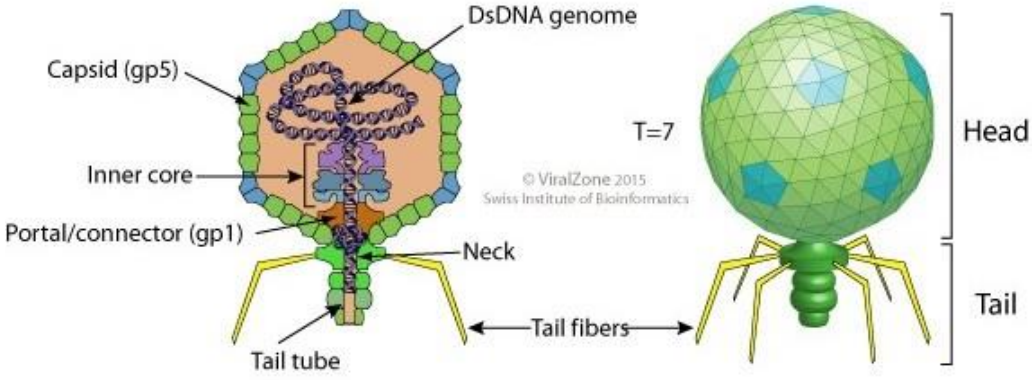

Figure 5 scheme of bacteriophage P22 with head and tail (ViralZone, 2015)

The procapsid of bacteriophage P22 consists mainly of two proteins, the 47 kDa coat protein (CP) providing the basic structure of the capsid and the 33kDa scaffolding protein (SP) playing an essential role in capsid formation. Together, 420 molecules of CP and around 300 molecules of SP assemble to form a T=7 procapsid as can be seen in **Figure 5**. However, only around 120 molecules of SPs seem to be required for the assembly in vitro. In the wild type of the phage, a portal protein in the capsid serves as entry for the DNA and further ejection proteins are incorporated making the phage infectious. For the DNA to enter the procapsid, the SPs leave the procapsid and conformational changes happen increasing the diameter of the capsid. The procapsid therefore starts with a diameter of around 58 nm while the final capsid has a diameter of around 61 nm. (Calendar, 2005)

1.3.2. P22 capsids for cargo packaging

The above-mentioned capsid is with its characteristics an ideal tool for cargo-protein packaging. To achieve that, a genetically engineered plasmid was created by O'Neil et al., 2011, only containing the genetic information of the CP and SP from the P22 phage. Since only the C-terminus of the SP interacts with the CP to enable capsid formation, the N-terminus can be truncated to a certain extent. This increases the space available in the procapsid, further giving the possibility to fuse a protein-cargo to its N-terminus. An additional thrombin cleavage site between the fused cargo-protein and the truncated SP (SP141) serves as a flexible linker, but also enables the proteolytic separation of the cargo from the SP141 if needed. The whole concept can be observed in the following **Figure 6**.

This concept might enable the incorporation of nearly every protein that fits into the capsid and can be successfully fused to the SP. A special challenge should be the incorporation of membrane proteins, such as reaction centers since they remain functional only in detergent.

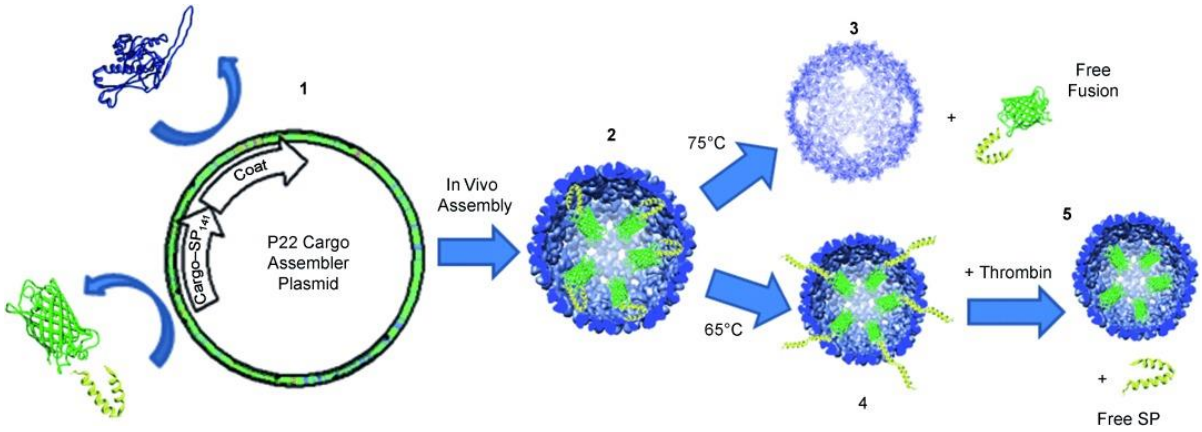

Figure 6 graphic explanation of the engineered concept; **1** plasmid with cargo-SP141 (green-yellow) and coat protein (purple) followed by in vivo assembly; **2** assembled capsid; **3** heating to 75°C leads to release of cargo-SP141 construct and expansion with holes in the capsid; **4** heating to 65°C leads to pre-release of SP141, complete release hindered by cargo **5** application of thrombin leads to proteolytic cleavage releasing SP141 and keeping cargo inside the capsid; (O'Neil et al., 2011)

2. Aims

1/ Establishing protocols for expression, isolation, and purification of P22 bacteriophage scaffolding and coat proteins of the viral capsid utilizing the plasmid P22_wtCP_SP141his.

2/ Establishing protocols for self-assembly of the P22 bacteriophage capsids *in vitro*.

3/ Establishing protocols for expression, isolation, and purification of photosynthetic reaction center complex RC-LH1 utilizing pIND4-RC1 plasmid and RCxr recipient strain of *Rhodobacter sphaeroides*.

4/ Fusing the H subunit of the RC-LH1 of *Rhodobacter sphaeroides* with scaffolding protein

5/ Isolation and purification of RC-LH1 with H subunit fused with P22 bacteriophage scaffolding protein.

6/ Assembly of P22 bacteriophage capsids with encapsulated photosynthetic reaction center complexes RC-LH1.

3. Materials and Methods

3.1. Reaction center expression and purification

3.1.1. Cultivation of *Rhodobacter sphaeroides* RC_x^r pIND4-RC1

Cells of *Rhodobacter* (*R.*) *sphaeroides* strain RC_x^r lacking the photosynthetic gene operon were transformed according to the protocol of Donohue & Kaplan, 1991. The midexponential phase cell culture was osmotically shocked by repeated dilution into ice-cold sterile deionized water and electroporated by a single pulse of 8.5 ms in a 2 mm electrode gap cuvette (400 ohm) at 2.5 kV, 25μF. The competent cells were transformed with plasmid pIND4-RC1 containing the photosynthetic gene operon with an engineered *puhA* gene with C-terminal histidine tag (Jun et al., 2014). Both the *R. sphaeroides* culture and the plasmid were a kind gift of Prof. J. T. Beatty (University of British Columbia, Vancouver, Canada). The culture was grown in RLB medium (Jun et al. 2014), supplemented with the antibiotic kanamycin at a concentration of 25 $mg.L^{-1}$. Isopropyl-beta-D-thiogalactopyranoside (IPTG) was added to the cultures to give a final concentration of 1 mM acting on the Lac-operon, thereby inducing expression of the reaction center proteins encoded in the pIND4-RC1 plasmid. The RLB medium was supplemented by Brunner's mineral medium microelement SL-4 and vitamin solutions (DSMZ GmbH, 2010). The cultures were grown at 30°C under illumination provided by incandescent light bulb. Aeration was provided by stirring and air bubbling.

The starting cultures of *R. sphaeroides* were prepared by inoculating 100 mL of RLB medium with a single colony grown on an RLB plate solidified by 15 % agar. These starting cultures were expanded to a volume of 1 L and then to 2 L. Following one week of growth in a 2 L bioreactor, the cells were harvested by centrifugation for 20 min at 4.200 rpm and 4°C. The obtained pellets were combined into 50 mL falcon flasks and shock frozen in liquid nitrogen. The flasks were stored at -80°C in the deep freeze until further use.

3.1.2. RC-LH1 complex purification

The 5 mL pellet of *R. sphaeroides* frozen at -80°C was melted on ice in the dark, subsequently resuspended in 15 mL of buffer A (10 mM Tris, 150 mM NaCl, pH 8.0) and homogenized by pipetting. An additional 35 mL of buffer A was added just prior to rupturing the cells in a LM-20 Microfluidizer (Microfluidics International Corporation, USA). At first, a pressure of 10.000 psi was used and then three additional times, a pressure of 25.000 psi was used. The solution with the broken cells was then centrifuged at 10.000g for 10 min at 4°C to pellet the

unbroken cells and cell walls of the ruptured cells. A 20% solution of DDM was added to the separated supernatant to get a final concentration of 2% DDM in order to solubilize the RC-LH1 complexes from the membranes. The membrane solution was then solubilized while stirred with a magnetic stirrer in the dark for 20 min. After 10 min imidazole is added to reach a final concentration of 5 mM. The solution was then centrifuged at 40.000 g for 30 min at 4°C. $MgCl_2$ was added to the supernatant in order to reach a final concentration of 0.5 mM like the buffer used in the template protocol (Jun et al., 2018).

The Econo-Column chromatography column (30x1.5 cm, Bio-Rad, USA) packed with Ni-NTA His Bind Resin (Merck Millipore, DE) was equilibrated with buffer B (buffer A, 0.03% DDM, 5 mM imidazole) using an EP-1 Econo Pump (Bio-Rad, USA). The solubilized sample was filtered using a 0.2 μm pore size hydrophilic filter, pipetted on the top of the column bed (15 mL per purification cycle) and the column was washed with 4 column volumes (100 mL) of buffer B at a flow rate of 1.5 $mL.min^{-1}$. The RC-LH1 complex was then eluted from the column by elution buffer (buffer B containing 150 mM imidazole). The elution was monitored by measurement of absorbance at 280 nm. Fractions collected in 2 mL tubes were analyzed by measurements of absorption spectra and separated using SDS-PAGE electrophoresis. At the end of the elution peak, the column was washed with 1 M imidazole, re-equilibrated with 5 column volumes of buffer B and new sample was loaded for purification.

The fractions with the largest ratio of absorbance of BChl a of the RC-LH1 complex (874nm) to the carotenoids at 472 nm were pooled, concentrated using 100kDa cut-off centrifugation filtration devices (centricon). Final purification was done with size exclusion chromatography (SEC) using a TSK Gel 6000 column, with 0.5 $mL.min^{-1}$ flow of a buffer containing 50 mM Tris pH 7.6, 150 mM NaCl and 0.03% DDM. The best fractions were pooled again and concentrated using centricons with 100kDa cut-off and stored in the dark at 4°C. Photosystem complexes concentration was measured on the base of BChl a concentration assuming 56 BChl a molecules per photosystem dimer. Concentration of the BChl a was assayed spectroscopically by absorbance measurements of the acetone extract utilizing a molar extinction coefficient E_{770nm} = 76.000 $M^{-1}cm^{-1}$.

3.2. P22 capsid protein expression and isolation

3.2.1. P22_wtCP_SP141his plasmid multiplication in *E. coli* DH5α and its purification

LB medium agar plates containing kanamycin were inoculated with a bacterial stab containing *Escherichia* (*E.*) *coli* DH5α with the P22_wt_SP141his plasmid carrying kanamycin (KM) resistance cassette purchased from Addgene (Plasmid ID#122651; **Figure 7**). After three days, the bacteria were transferred from the petri dish to liquid Luria-Bertani (LB) medium and put in a shaker at 37°C and 180 rpm. A day later, the plasmid was isolated and purified using a NucleoBond® Xtra Midi DNA isolation kit (Macherey-Nagel, DE).

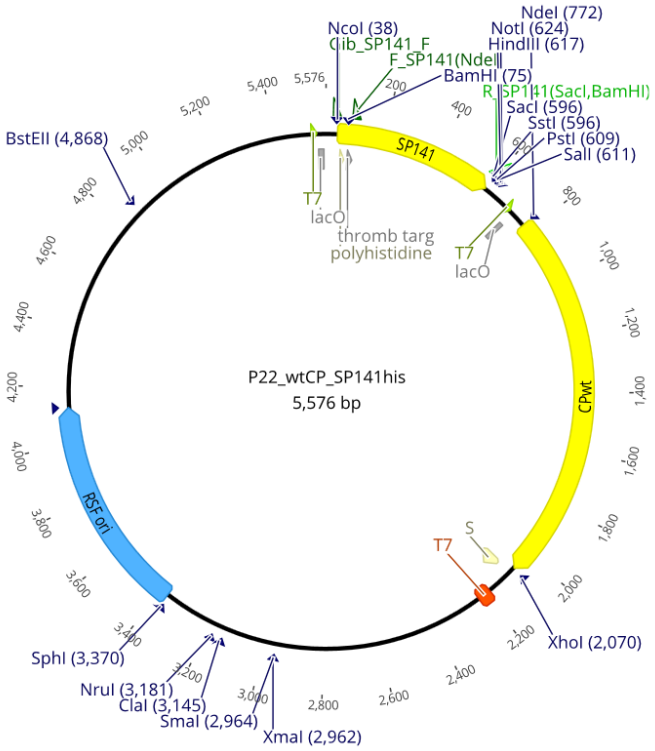

Figure 7 P22_wtCP_SP141his plasmid scheme from Genious Prime

Thereby, 100 mL of bacterial suspension was transferred into two 5 mL tubes and centrifuged at 8.000 rpm for 15 min. The supernatant was discarded, and the pellet was resuspended in 8 mL buffer containing RES and RNAse solutions. The whole solution was homogenized with a vortex. Then, 8 mL lysis buffer was added, the tube was flipped and let stand for 5 min. After this, the filtration cartage from the kit was wetted using 12 mL EQU buffer. Then, 8 mL of NEU buffer was added to the sample turning the solution blue. The solution was gently flipped 3 times and then poured into the cartridge. An additional 5 mL of EQU buffer was added to wash the cartridge. After the cartage was taken out, 8 mL of wash buffer were poured onto the

collection tube. Then, 10 mL of ELU elution buffer was added to release the DNA out of the column. The flow through was collected into a 15 mL falcon tube. To that, 5 mL of iso-propanol was added, the solution was vortexed and then centrifuged at 4°C and 15.000g for 30 min. After the centrifugation, the supernatant was discarded and the pellet was washed and then centrifuged two times using 70% ethanol, while discarding the supernatant after every centrifugation. The washed pellet was dried for 3 hours and then rehydrated using 200µL PCR water and the P22_wtCP_SP141his plasmid DNA concentration was measured using NanoDrop. The rehydrated plasmid solutions (#2GW - 274.0 ng.µL^{-1}, #1DK - 485.2 ng.µL^{-1}) were aliquoted and stored in the freezer at -20°C.

3.2.2. Transformation of *E. coli* BL-21 (DE3) with P22_wtCP_SP141his plasmid

Stock suspension of *E. coli* BL-21 (DE3) (New England Biolabs Inc., USA) production strain was taken out of the -80°C deep freezer and melted on ice. One µL of the aliquot of the P22_wtCP_SP141his master plasmid stock solution diluted with ultrapure water to a concentration of 50 ng of DNA per µL^{-1} was added to the *E. coli* BL-21 (DE3) suspension. The tube was flipped 4-5 times carefully and kept for 30 min on ice without mixing. The solution was heat shocked afterwards in a water bath at 42°C for exactly 10 s and not mixed. 250 µL of SOC medium were added, the solution was inverted a few times and put on a shaker for 1 hour at 37°C and 300 rpm. In the end, an agar plate containing LB medium supplemented with KM (50 mg.L^{-1}) was inoculated with 50 µL cell suspension and placed into an incubator at 37°C. KM was added to the rest of the cell suspension to the final concentration of 50 mg.L^{-1} and it was kept in the fridge overnight.

On the next day, 20 glycerol stocks containing *E. coli* suspension were prepared for later use. Therefore, 750 µL of *E. coli* in LB medium and 250 µL of 60% glycerol solution was mixed together in a tube and aliquots were shock-frozen in liquid nitrogen. The shock frozen cells were then stored in the deep freezer at -80°C. The rest of the *E. coli* cell culture was used for subsequent pilot expression.

3.2.3. Pilot expression of P22 capsid proteins

E. coli BL-21 (DE3) cell suspension transformed with P22_wtCP_SP141his plasmid (300 µL of cell solution, corresponding to the final optical density at 600nm wavelength (OD_{600}) of 0.1) was inoculated into two culture tubes containing 10 mL of LB medium supplemented with KM (50 mg.L^{-1}). Culture tubes were put in a shaker at 37°C and 180 rpm. One mL of

sample was taken from the control and the expression flask at several timestamps to monitor the growth using the measurements of OD_{600} and later the qualitative protein level expression using the SDS-PAGE electrophoresis. Cell suspension incubation proceeded until an OD_{600} of around 0.4 was reached. At that point, IPTG was added to the expression cultivation flask to a final concentration of 1 mM. The 1 mL samples were centrifuged for 2 min at 14.000 rpm, the supernatant was discarded, and the samples were stored in the freezer at -20°C for further analysis on SDS-PAGE.

The frozen pellets of the samples collected for SDS-PAGE analysis were resuspended by addition of 150 µL lysis buffer and vortexed. Samples were then incubated on a heat block at 95°C for 2 min, vortexed and frozen in liquid nitrogen. The last three steps were repeated 4 times. At the end, samples were placed again on the 95°C heat block for 2 min, centrifuged at 15.000 rpm for 2 min and the supernatants were transferred to separate tubes. To prepare the samples for the loading on the gel, 50 µL of 4x SDS-buffer were added to the tubes containing the supernatant or so-called soluble fraction (~150 µL) and 150 µL of 1x SDS-buffer were added to the tubes containing the pellet or so-called non-soluble fraction. 10 µL of each sample were loaded on the gel, 5 µL of the protein ladder. 15% acrylamide SDS-PAGE gel was used since the scaffolding protein (SP141) has a molecular weight of 20.295 kDa and the coat protein (wtCP) of 46.751 kDa. The gel was run for 90 min with 100V through the stacking gel and 180V through the running gel.

3.2.4. Mass production of P22 capsid proteins

For the mass production, six large scale cultivation flasks were used, containing 800 mL of LB medium and 800 µL of KM stock (50 $mg.mL^{-1}$). The large-scale cultivation flasks were then inoculated from an overnight grown starter culture of *E. coli* BL21(DE3) cells carrying the plasmid P22_wtCP_SP141his. After inoculation the cultivation flasks were placed in a shaker for growing at 37°C. The OD_{600} was monitored every 20 min till an OD_{600} of around 1 was reached. As OD_{600}=1 was reached after 80 min, the production of SP141 and CPwt proteins was induced by pipetting 800 µL of IPTG (1M stock, final concentration in the cell culture 1 mM) into the cultivation flask and the cells were grown for another 4 hours. After those 4 hours, the cells were pelleted by centrifugation for 20 min at 4.200 rpm and 4°C, the supernatant was removed (decontaminated and discarded), and the pellets combined into a 50 mL falcon tube. The tube with cell pellet was frozen in liquid nitrogen and stored at -80°C till further use.

A 1 mL sample from two flasks was taken just before the induction and after 4 hours of additional growing. These samples were centrifuged for 2 min at 14.500 rpm, the supernatant was discarded, and the pellet was frozen. On a separate day, the pellet of the samples was processed the same as in "Pilot expression of P22 capsid proteins" to obtain a clear separation of the expressed proteins on the SDS-PAGE.

3.2.5. Capsid purification using rate zonal sucrose gradient centrifugation and SEC chromatography

The purification was done similar to O'Neil et al., 2011. Frozen cells from the mass production were thawed from -80°C and resuspended in buffer α (150mM NaCl, 50mM Tris-HCl, pH 7.6) with the addition of DNAse with a final concentration of 10 $\mu g.mL^{-1}$ and RNAse with a final concentration of 50 $\mu g.mL^{-1}$. The resuspended solution was homogenized using a LM-20 Microfluidizer (Microfluidics International Corporation, USA), by passing the solution 2 times at 10.000 psi and 3 times at 20.000 psi through the press. The obtained ~50 mL of cell lysate was centrifuged at 10.000g for 1 hour in a Sigma centrifuge to remove the cell debris. The supernatant was pelleted in a Beckmann ultracentrifuge at 45.000 rpm for 2 hours using a 70Ti fixed angle rotor. After removing the supernatant, the pellet containing the virus like particles (VLPs) was resuspended in 30 mL of buffer β (buffer α + 1mM EDTA). Two mL of this suspension were carefully loaded on top of a 5-20% sucrose gradient on basis of buffer β and centrifuged in a SW 40 Ti swing out rotor at 35.000 rpm for 30 min. A milky opalescent band in the middle of the tube height was collected and pelleted in a 70 Ti fixed angle rotor at 45.000 rpm for 1 hour. The pellet of the milky band was resuspended in the smallest possible volume of buffer β and purified with size exclusion chromatography using TSK Gel 6000 column, with 0.5 $mL.min^{-1}$ flow of a buffer β. The fractions containing the purified VLPs were pooled.

Scaffolding protein was extracted from the VLPs by incubating them in a buffer β with the addition of 0.6 M guanidine-HCl at room temperature for 1 hour. This reaction solution was then centrifuged in a Beckmann ultracentrifuge at 45.000 rpm for 2 hours using a 70Ti fixed angle rotor. The supernatant containing SP141 protein was concentrated in centricon with 10 kDa cut-off. The pellet containing the empty shells composed of coat protein CPwt was resuspended in 3 mL of buffer β.

Protein concentrations were measured spectroscopically at 280 nm in NanoDrop using molar extinction coefficient of E_{SP141}=13.075 $M^{-1}cm^{-1}$ and E_{CPwt}=44.920 $M^{-1}cm^{-1}$. Protein purity was assayed by separating the protein solutions using SDS-PAGE electrophoresis.

3.3. Modification and purification of scaffolding protein (SP141)

3.3.1. Genetic modification of SP141his for thrombin cleavage

Following the original sequence annotations of the P22_wtCP_SP141his plasmid, the translated SP141 protein should contain N-terminal histidine Tag (His-Tag) followed by a thrombin cleavage site designed to cleave off the His-Tag. Control sequencing of the plasmid revealed that this thrombin cleavage site was out of frame and therefore not present in the translated protein. To cleave off the His-Tag for further manipulations, the SP141 sequence had to be changed to restore the thrombin cleavage site. This was done by amplification of the SP141 sequence using PCR but leaving out the 5' end containing the His-Tag and out-of-frame thrombin cleavage site. An *Nde1* restriction site was added to the overhang of the forward primer (F_SP141(Nde1); 5'-GGCAGCCATATGTGTCGCAGCAATGCCGTA-3') and a *BamH1* and *Sac1* restriction site were added to the overhang of the reverse primer (R_SP141(Sac1, BamH1); 5'-TCTCTCGAGCTCGGATCCTTATCGGATTCCTTTAAGT-TTTGC-3'). The PCR reaction was done with Q5 polymerase and was mixed like in the following **Table 1**:

Table 1 reaction mixture to amplify SP141 fragment for cloning into pET15b

Reaction buffer 5x	10 µL
dNTPs (10 mM; 2.5 mM each)	1 µL
Forward primer F_SP141 (10 µM)	2.5 µL
Reverse primer R_SP141 (10 µM)	2.5 µL
Q5 polymerase	0.5 µL
GC enhancer	10 µL
P22_wtCP_SP141his (50 ng/µL)	1 µL
PCR H_2O	22.5 µL
TOTAL	50 µL

This mixture was incubated in a PCR cycler using the protocol from **Table 2**:

Table 2 PCR cycler program of SP141 amplification

	30sec	98°C
35x	10sec	98°C
	30sec	62°C
	25sec	72°C
2min		72°C

The obtained product was separated by horizontal electrophoresis using a 1% agarose gel. The band of approximately 500bp is length was cut out of the gel and then cleaned using the gel cleaning kit (Macherey-Nagel, DE). The DNA concentration of the obtained PCR product was measured in NanoDrop (SP141_new: 187.9 $ng.\mu L^{-1}$).

The ends of the SP141 PCR-fragment were cleaved by the *Nde1* and *Sac1-HF* restriction enzymes to ligate the fragment in the open pET15b plasmid. The reaction was mixed like in the following **Table 3** and incubated for 15min at 37°C in a PCR cycler. After incubation, the mixture was cleaned using a PCR cleaning kit (Macherey-Nagel, DE) and its concentration was measured on NanoDrop (SP141_new_cut: 28.1 $ng.\mu L^{-1}$).

Table 3 restriction of SP141 PCR-product for ligation into pET15b plasmid

10x CutSmart Buffer	5 µL
NdeI	1 µL
SacI-HF	1 µL
SP141_new 1 µg	5.32 µL
H_2O	37.68 µL
TOTAL	50 µL

For the ligation, an open pET15b plasmid with *NdeI* and *SacI* overhang provided by Dr. Paulina Duhita Anindita from our team was used to insert the cut SP141 PCR-fragment. It was inserted just behind the His-Tag and thrombin cleavage site of the given plasmid. The reaction was mixed following the composition in **Table 4** and incubated at 16°C overnight.

Table 4 ligation reaction of SP141 fragment into pET15b plasmid

	volume	length	concentration	mass
10x T4 DNA Ligase Buffer	2 µL			
Linearized vector **pET15b_res.**	2.47 µL	5 kb	20.2 $ng.\mu L^{-1}$	50 ng
Digested insert **SP141_new_cut.**	0.53 µL	522 bp	28.1 $ng.\mu L^{-1}$	15 ng
T4 DNA Ligase	1 µL			
H_2O	14 µL			

The 5’ end of SP141 before and after fixing the thrombin site can be observed in the following in silico schemes (**Figure 8**; **Figure 9**) from Geneious Prime:

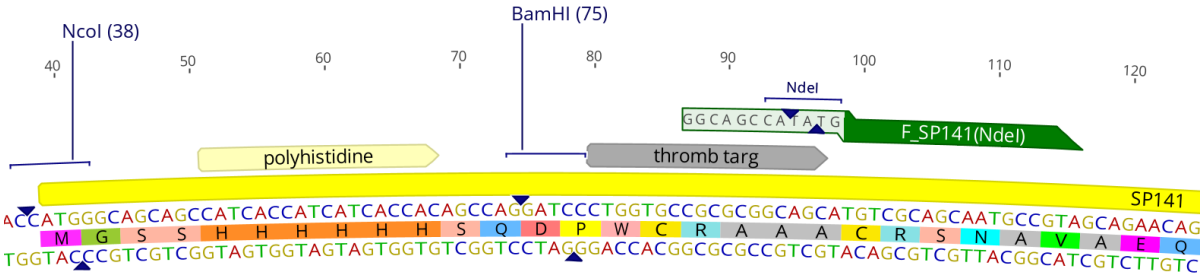

Figure 8 5' end of SP141his on P22_wtCP_SP141his plasmid with out-of-frame thrombin site

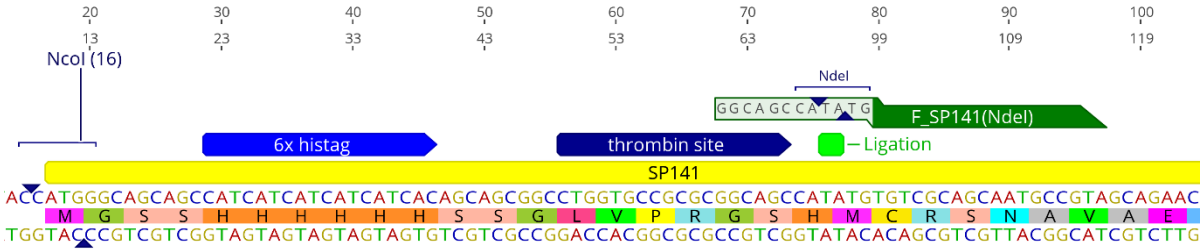

Figure 9 5' end of SP141thromb on pET15b_SP141thromb plasmid with in-frame thrombin site

After ligation, 2 µL reaction mixture containing the new plasmid (pET15b_SP141thromb) was used to transform *E. coli* DH5α competent cells (New England Biolabs Inc., USA) that were thawed on ice. Therefore, the reaction mixture was carefully added to the cells, and the tube was flicked several times. That mixture got placed on ice for 30 min without mixing, then heat shocked at 42°C for 30 seconds, and placed again on ice for 2 min. To that, 950 µL of SOC media was added that got heated to room temperature and the mixture was incubated at 37°C on a shaker (250 rpm) for 60 min. During the incubation, selection plates containing ampicillin were warmed to 37°C. 100 µL of the cells got then spread on the selection plates and incubated overnight at 37°C.

On the next day, colony PCR was performed with some of the obtained colonies. The rest of the solutions containing the picked colonies with positive colony PCR were used to inoculate flasks with 5 mL LB medium and 50 $mg.L^{-1}$ kanamycin (KAN). These flasks were incubated overnight at 37°C on a shaker and the plasmids were isolated on the next day using NucleoBond® Xtra Midi DNA isolation kit (Macherey-Nagel, DE) and the DNA concentration was measured using NanoDrop.

3.3.2. Expression and purification of SP141thromb

To prepare the cells directly for mass production, 2 µL of isolated pET15b_SP141thromb plasmid solution (#10; 49.0 ng.µL^{-1}) were used to transform *E. coli* BL21(DE3) using the same protocol as for the *E. coli* DH5α after ligation. The obtained plates were grown overnight and one colony was used to inoculate a flask containing 5 mL LB medium and 50 mg.L^{-1} KAN. That flask was grown at 37°C for several hours on a shaker, further expanded to 100 mL using the same LB+KAN medium and grown overnight.

The mass production was then performed analogously to the mass production of P22 capsids in chapter 3.2.4. , the cells were stored at -80°C and the collected samples were analyzed on 15% SDS-PAGE.

For purification, the SP141his containing *E. coli* from mass production were thawed from -80°C. The thawed cells were resuspended in 25 mL of buffer EQ (150 mM NaCl; 10 mM Tris; pH 7.6). This suspension was put through a French press for 2 times at 10.000 psi and 3 times at 20.000 psi. The obtained cell lysate was then centrifuged at 4°C and 40.000g for 1 hour. After centrifugation, the pellet was discarded, and the supernatant collected for further use. During centrifugation, a 5 mL HisTrap^{TM} HP column (Cytiva, USA) was equilibrated using buffer EQ. After equilibration, 50 mL of the collected supernatant were loaded onto the column. The column was then washed using buffer EQ till no apparent proteins (based on absorption at 280 nm) came out anymore. The column was then washed with buffer EQ mixed with 30% buffer EL (buffer EQ + 0.5 M imidazole), leading to a 150 mM imidazole wash. Washing was followed by elution of the bound protein by buffer EL. The eluted protein was collected in fractions that were analyzed on 15% SDS-PAGE. The fractions containing SP141thromb were combined and dialyzed using a 3kDa cut-off centricon and shrunk to a volume of 150 µL, to increase concentration and remove imidazole.

3.3.3. Cleavage of HisTag from SP141 using thrombin

To prepare the SP141 protein for the reaction with the NTA-linker, its His-tag needs to be removed. Since SP141 contains a thrombin cleavage site behind the His-tag, it could be removed using the enzyme thrombin. In this case, 1U of thrombin per 1 mg of SP141 protein were used. Proper enzyme activity of thrombin was enabled by adding $CaCl_2$ to a final concentration of 5mM. Then, the reaction ran for 15 min on ice. To stop the reaction, 1 M PMSF was added to reach a final concentration of 1 mM. After that, the solution was loaded on a 1 mL HisTrap^{TM} HP column (Cytiva, USA). The column was equilibrated with 10 mL of

buffer EQ (150mM NaCl, 10mM Tris, pH 7.6), then the ~3.5 mL of sample were loaded, the column was washed with 2 mL of buffer EQ and then eluted with 4 mL of buffer EL (buffer EQ + 0.5 M imidazole). Five 1 mL fractions were taken during loading and washing, and three 1 mL fractions were taken during elution. The fractions were analyzed on a 15% SDS-PAGE.

The 3 fractions of SP141 from the elution were combined and concentrated on a 3 kDa cut-off centricon at 6.000 rpm and 4°C. A final volume of 730 µL was reached that was further concentrated to 600 µL on a 1 kDa cut-off centricon at 6.000 rpm and 4°C for 15min. The concentration of obtained SP141 solution was measured on NanoDrop (61.745 µM) and got then used for coupling with a NTA-maleimide linker.

3.3.4. Linkage of cleaved SP141 to NTA-maleimide-linker

The SP141 was linked to NTA-maleimide serving as linker following a manual by Hermann J. Gruber, Institute of Biophysics at Johannes Kepler University. (Gruber, n.d.)

To the SP141 solution obtained in the previous step, 3 mL of 50 mM Hepes, 70 µl of 100 mM EDTA (pH 7.5) and 70 µl of 100 mM TCEP hydrochloride were added in that specific order. Between each addition, the sample was well mixed. During the last addition, the pH decreases from 7.5 to 7.2 and by final addition of 70 µl of 1 M Hepes (pH 9.6) the pH raises to about 7.6.

Because the sample still contained imidazole from elution, the sample was dialyzed by centrifugation using the 1 kDa centricon at 6.000 rpm and 4°C, and addition of 1 mM Tris and 50 mM Hepes containing buffer. After a 16x dilution of the imidazole was reached and the sample was concentrated to 1250 µL, 125 µL of NTA-maleimide linker (10 mM) were added to the sample. The reaction took 2 hours and was performed at room temperature. With the obtained product, SEC was performed analogous to 3.2.5. to separate the SP141-NTA product from side products and unreacted educts. The first two fractions were combined and analyzed using NanoDrop.

Protein mass was determined using MALDI-TOF/TOF mass spectrometer (MS) Autoflex (Bruker Daltonik, USA) by Dr. Filip Dyčka. Prior the MS experiment, the proteins were purified using C4 or C18 ZipTip (Merck, DE). The intact protein (0.5 µL) was spotted on the MALDI target and mixed with the same volume of matrix. Two different matrices were used: 10 $mg.mL^{-1}$ alpha-cyano-4-hydroxycinnamic acid (CHCA) and 30 $mg.mL^{-1}$ sinapinic acid dissolved in acetonitrile/0.1% TFA in a volume ratio 7:3. Mass spectra were acquired in the

positive linear ion mode using pulsed extraction with an acceleration voltage of 19.5 kV, an extraction voltage 18.2 kV, a len voltage of 7 kV and delayed extraction time of 360 ns. Resulting spectra were accumulated from up to 500 laser shots. Mass spectra processing was performed using flexAnalysis 3.4 (Bruker Daltonik, USA).

3.4. Capsid assembly with reaction center RC-LH1

At first, the reaction center complex (RC-LH1) was coupled with the SP141-NTA through the His-Tag of its H subunit (**Figure 25**, 2nd reaction), to enable the incorporation of the RC-LH1 into the capsid. This was done by mixing 20 µL of SP141-NTA (61.7 µM) with 350µL RCLH1pufX dimer (2.34 µM) and 0.4 µL of 1 M $NiCl_2$. A ratio of 10:1 between SP141 and SP141-NTA-RCLH1 was chosen to enable proper capsid formation. This solution was then used to mix the final reaction in a way that 36 µM wtCP, 15µM SP141 and 1.5µM SP141-NTA-RCLH1 (20:10:1) were present in the solution. The obtained product was then observed using an electron microscope by our doctoral student Eva Ďurinová. Samples were deposited on glow-discharged carbon-coated copper grids and negatively stained with 1.5% uranyl acetate and visualized using a JEOL JEM-2100F transmission electron microscope (JEOL, Tokyo, Japan; using 200 kV at 20,000 × magnification). TEM images were recorded using a bottom-mounted Gatan CCD Orius SC1000 camera, with a resolution corresponding to 3.4 Å per pixel.

4. Results

4.1. Reaction center RC-LH1 purification

A representative chromatogram of the performed purifications can be observed in **Figure 10**.

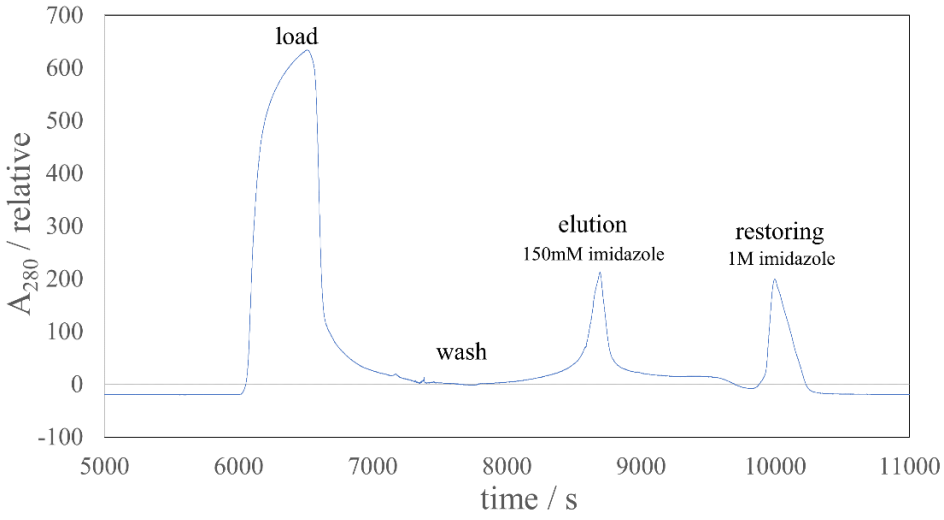

Figure 10 exemplary chromatogram from HisTag affinity chromatography of RC-LH1. Showing load, wash, elution and restoring of column

The first large peak represents the load, followed by washing. The elution of the RC-LH1s with buffer contained 150 mM imidazole is signalized by a sharp peak ("elution") where several fractions got collected. The "restoring" peak caused 1M imidazole was probably due to other bound proteins, smaller than the RC-LH1 and therefore better interacting with the column. The measured absorbance spectra of the eluted fractions were used to identify the peak fractions that can be observed in **Figure 11**.

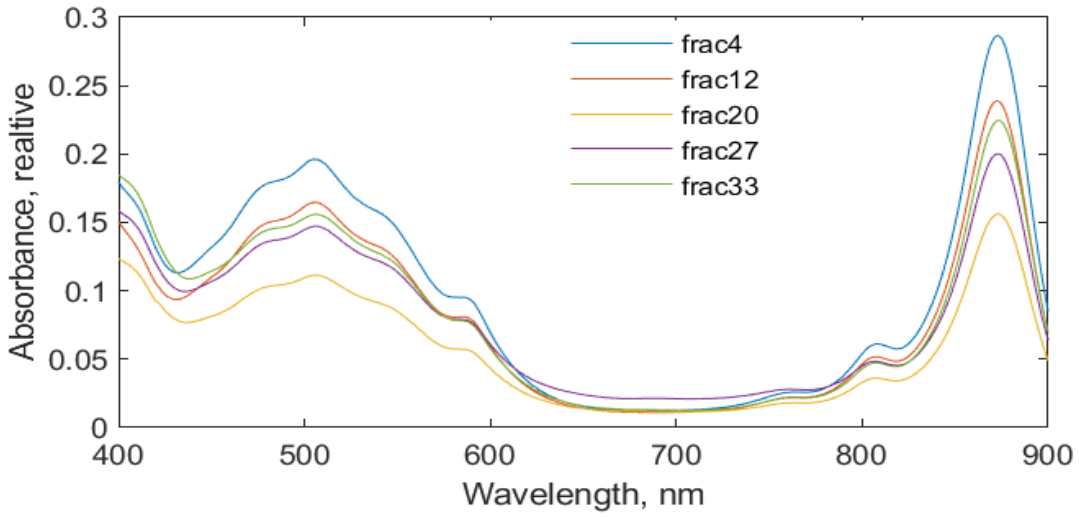

Figure 11 measured spectra of peak fractions from RC-LH1 purifications on HisTag column

The ratio between the peak at 870 nm and 510nm can be used to evaluate the purity of the reaction centers. In this case a ratio above 1 can be observed for all peak fractions, indicating a high purity of the reaction centers, which can thereby be used for further analysis.

The SDS-PAGE in **Figure 12** shows the purified RC-LH1 with its RC-subunits H, M and L as well as the other proteins present in the LH1 such as pufX and the α and β subunits of the LH1. The assignment of the RC-subunits was confirmed by MS measurements.

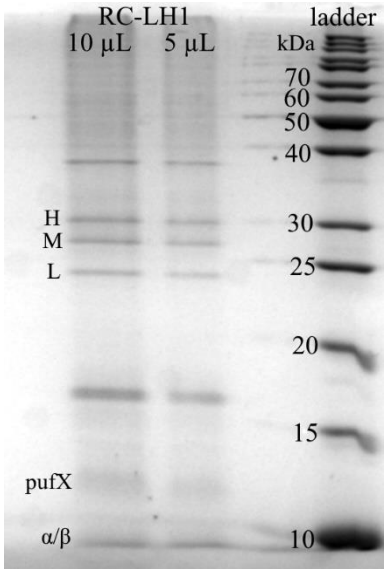

Figure 12 SDS-PAGE of RC-LH1 with labelled building blocks, first two lanes with RC-LH1 (10µL;5µL);3rd lane marker leakage; 4th 5µL ladder; stained with Coomassie blue

4.2. Expression of capsids in E. Coli BL-21 (DE3)

4.2.1. Pilot expression of capsids

The pilot expression of the viral capsids in *E. coli* can be observed on the 15% SDS-PAGEs with insoluble fraction in **Figure 13** and soluble fraction in **Figure 14**. Since the coat protein (wtCP) has a molecular weight of around 46.8 kDa and the scaffolding protein (SP141his) of around 20.3 kDa, judging from the SDS-PAGE, the wtCP can be found especially in the insoluble fraction and the SP141his especially in the soluble fraction. It can be observed that the corresponding bands (20.3 kDa, soluble; 40.6 kDa, insoluble) thicken after induction with IPTG suggesting a good expression, compared to the non-induced sample. The capsids should therefore be found in the insoluble fraction and mass production can be performed.

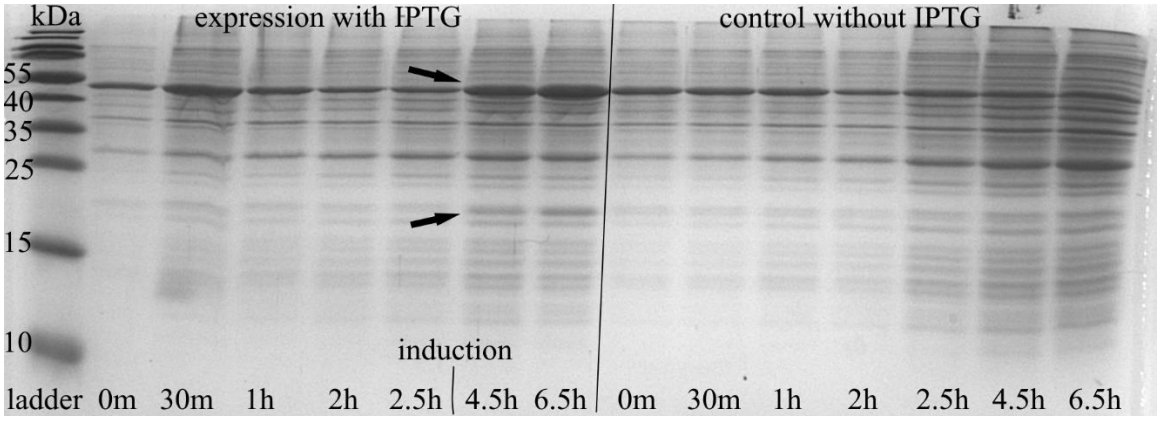

Figure 13 SDS-PAGE of pilot expression. The insoluble fraction showing the expression with IPTG on the left side, and the control without ITPG on the right side. Induction with IPTG after 2.5h (OD_{600}=1 at t=2.5h); ladder (5µL) in first lane, samples (10µL) in 2nd-15th lane; stained with Coomassie blue

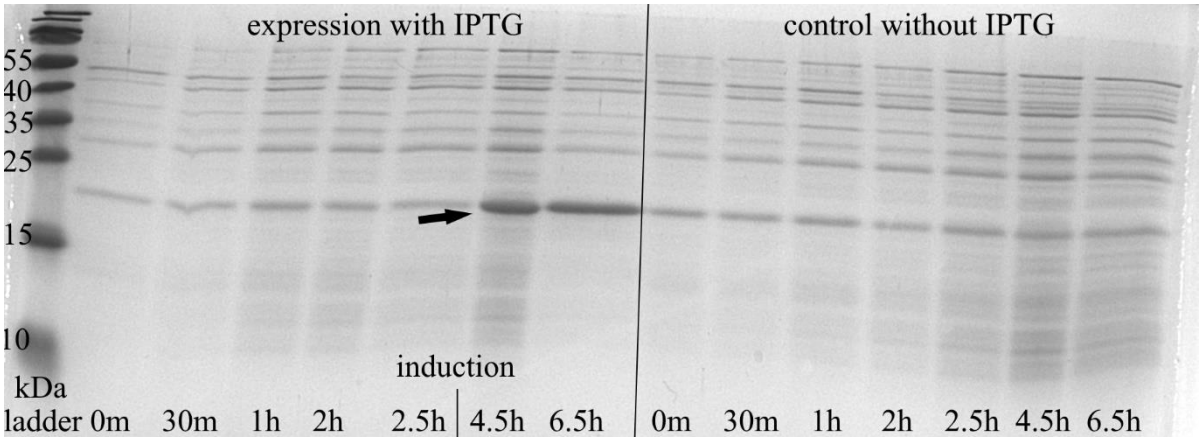

Figure 14 SDS-PAGE of pilot expression. The soluble fraction showing the expression with IPTG on the left side, and the control without ITPG on the right side. Induction with IPTG after 2.5h. Time noted from culture start (OD_{600}=1 at t=2.5h); ladder (5µL) in first lane, samples (10µL) in 2nd-15th lane; stained with Coomassie blue

4.2.2. Mass production of capsids

The mass production of the capsids can be observed on the 15% SDS-PAGE in **Figure 15**. Both expressed proteins forming the capsids, SP141 and wtCP, can be found again in the insoluble fraction confirming the assumption from the pilot expression that the capsids can be found there. In addition, the majority of SP141 being present in the soluble fraction, with no wtCP being found there, suggests an overproduction of SP141 in relation to wtCP. Therefore, it should be possible to isolate the SP141 protein from the soluble fraction if needed, without eluting them from the assembled capsids.

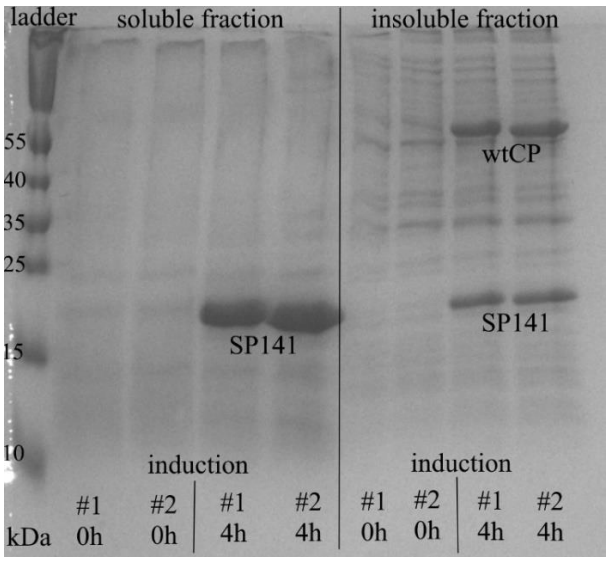

Figure 15 SDS-PAGE monitoring mass production of capsids. Soluble fraction of flask #1 and #2 on the left side. Insoluble fraction on the right side. Time noted starting at induction with IPTG (OD_{600}=1 at t=0h); ladder (5µL; 1st lane), samples (10µL; 2nd-9th lane); stained with Coomassie blue

4.2.3. Capsid purification

In the following, the capsid purification on SEC after sucrose gradient can be observed. The milky band after sucrose gradient was loaded and ten 0.5 mL fractions were collected around and after the peak (**Figure 16**, right). These fractions (A-J) were run on a 15% SDS-PAGE (**Figure 16**, left) and the four fractions with highest intensity (B-E) also corresponding to the peak on the chromatogram got pooled.

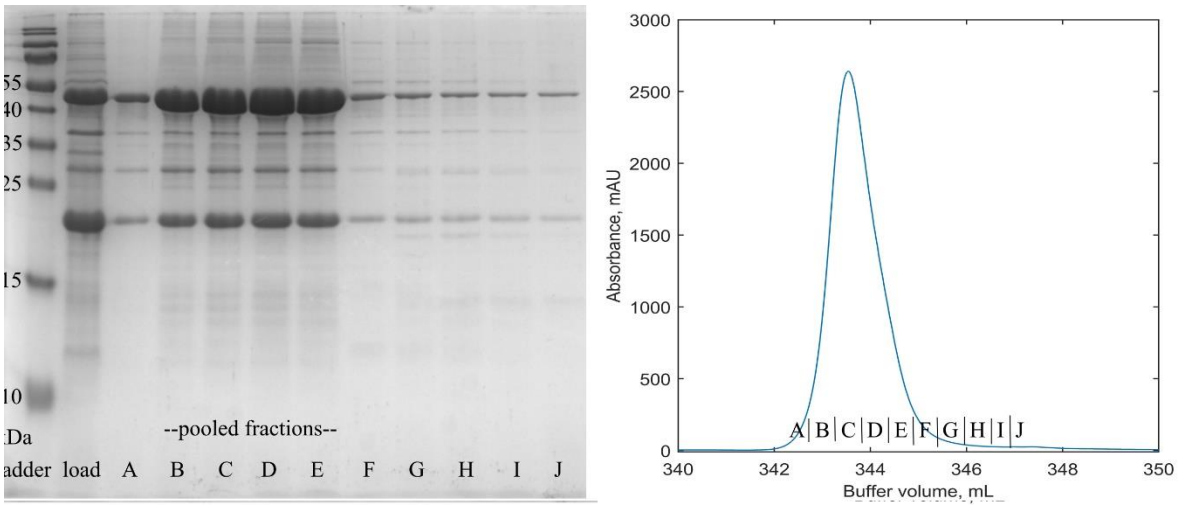

Figure 16 SDS-PAGE after SEC of capsids; ladder (1st lane; 2µL); load (2nd lane; 2µL); fractions A-J (3rd-10th lane; 2µL) stained with Coomassie blue (left) and chromatogram of the same SEC with marked fractions (right)

4.3. Modification and purification of scaffolding protein (SP141)

4.3.1. Genetic Engineering of SP141

After successful PCR of the SP141 gene from the P22_wtCP_SP141his plasmid, the following agarose gel was obtained (**Figure 17**) using newly designed primers:

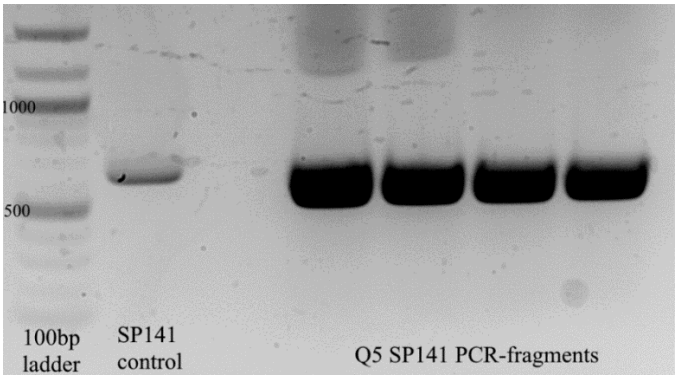

Figure 17 1% agarose gel after PCR of SP141 fragment (15µL, lane 4-7); 100bp ladder (15µL, lane 1); SP141 control originated from previous experiments (15µL, lane 2); gel stained with Sybre green

From that gel, the 522bp SP141 PCR-fragment was cut out, purified, and used for insertion into the newly designed pET15b_SP141thromb plasmid. Transformation of *E. coli* DH5α with that plasmid and successful colony PCR can be observed on the following gel (**Figure 18**). Following that, the 10th colony was used for plasmid isolation and further transformation of the production strain used for mass production.

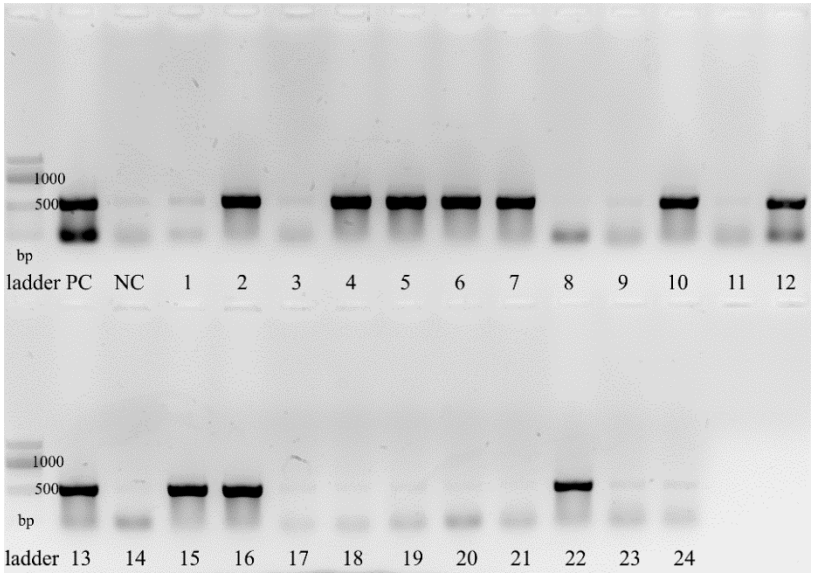

Figure 18 colony PCR after transformation of *E. coli* DH5α with newly created construct; PC = positive control (15µL; reaction mix + P22_wtCP_SP141his plasmid); NC = negative control (15µL; only reaction mix); picked colonies 1-24 (15µL each); stained with Sybre green

4.3.2. Expression and purification of SP141thromb

After transformation of the production strain (*E. coli* BL21(DE3)), mass production could be performed leading to the following SDS-PAGE (**Figure 19**):

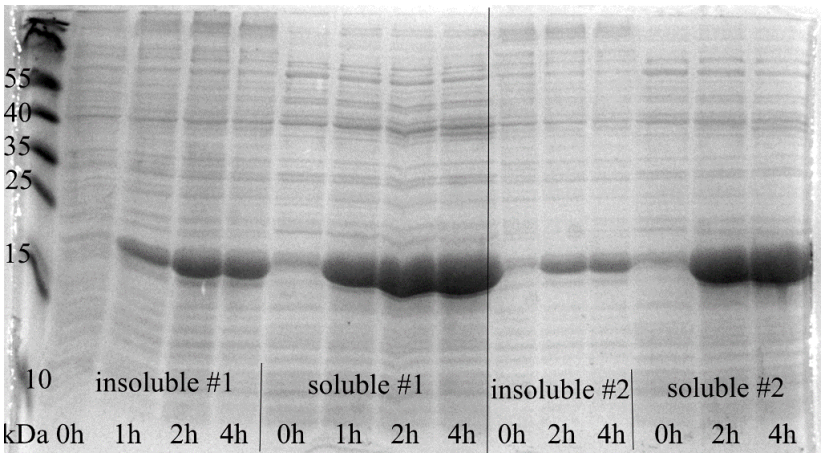

Figure 19 15% SDS-PAGE from mass production of SP141thromb with *E. coli* BL21(DE3) containing pET15b_SP141thromb plasmid; time taken after induction with IPTG (OD_{600}=1 at t=0h); ladder (5µL; 1st lane), 1# flask (10µL; 2nd-8th lane), 2nd flask (10µL; 9th-14th lane); stained with Coomassie blue

As can be seen, induction with ITPG lead to a good production of new SP141thromb (~20 kDa) protein in the soluble, but also insoluble fraction, that could be used now for HisTrap purification. The chromatogram of that purification is depicted in the following **Figure 20**:

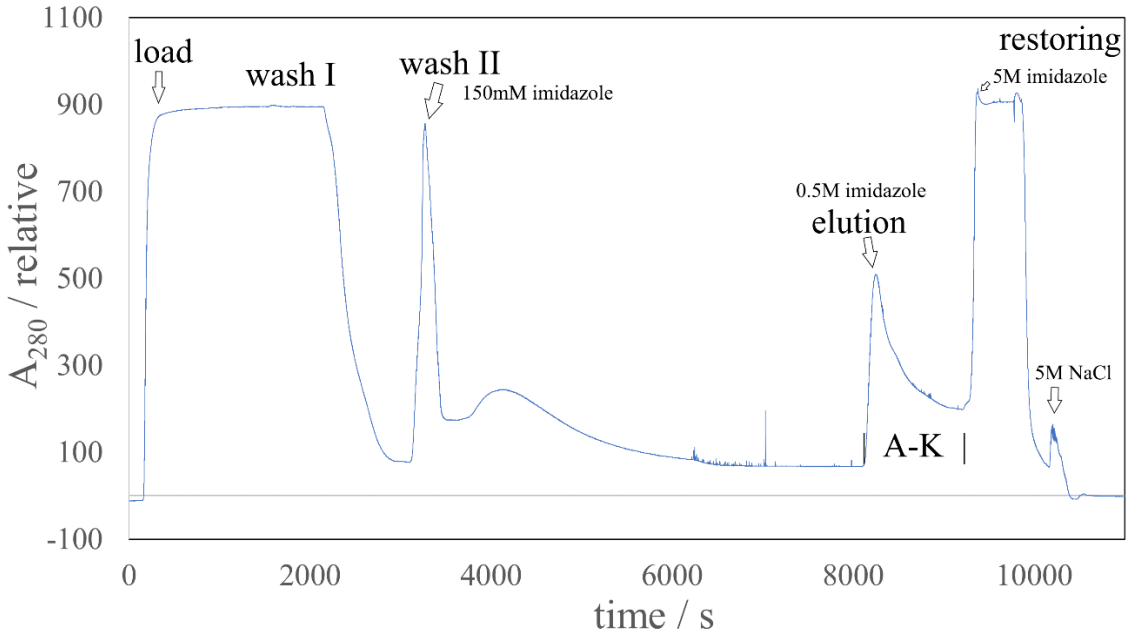

Figure 20 chromatogram of SP141thromb HisTrap purification with load, washI, washII, elution with collected fractions and restoring

The composition of the loaded sample, the proteins not binding to the column – flowthrough material (washI) and the proteins washed from the column by buffer containing 150 mM imidazole (washII) followed by the collected fractions around the elution peak can be observed on the following 15% SDS-PAGE (**Figure 21**):

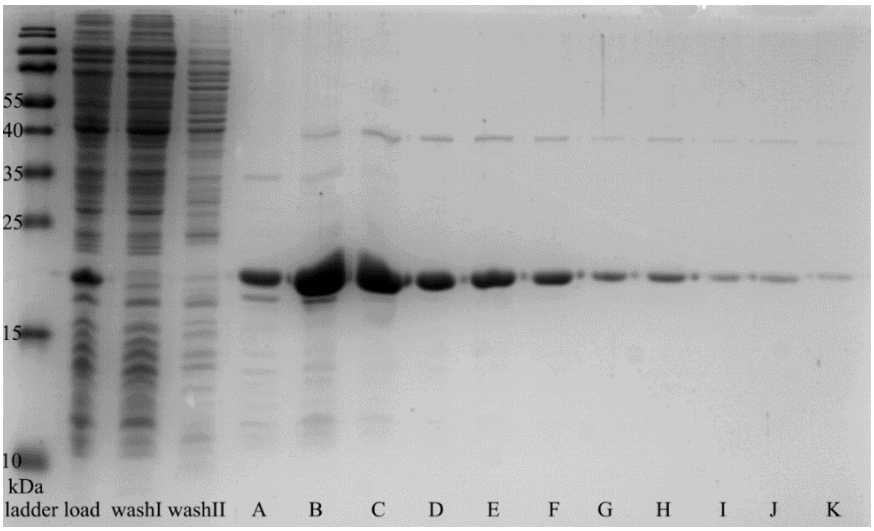

Figure 21 HisTrap column purification of SP141thromb with fractions A-K (5µL; 5th-15th lane); ladder, load, washI and washII (5µL; 1st-4th lane); stained with Coomassie blue

Since nearly all impurities got removed, following the difference between load and fractions, all collected fractions containing SP141thromb (fractions A-K) got pooled together. This was done despite the fact that fractions B and C contained most of the protein, to achieve a high yield and not waste the other fractions.

4.3.3. Thrombin cleavage of SP141

On the SDS-PAGE in **Figure 22**, it can be observed that the thrombin didn't only cleave the SP141 at the expected site (LVPR/GS) behind the HisTag, but also on a different site. When looking at the amino acid sequence of the protein *in silico*, one can find a second cleavage site with less specificity (LKPR/GK). The uncut protein has a molecular weight of around 20.3 kDa. Cleavage in the main site would result in a protein of around 18.4 kDa and in both sites in a protein fragment of around 12.8 kDa based on the in-silico sequence. This can be well observed on this SDS-PAGE, showing a slightly downshifted band at around 18 kDa indicating a cleaved-off HisTag. The second light band above 10 kDa matches the assumption that cleavage at both sites results in a protein fragment of around 12.8 kDa.

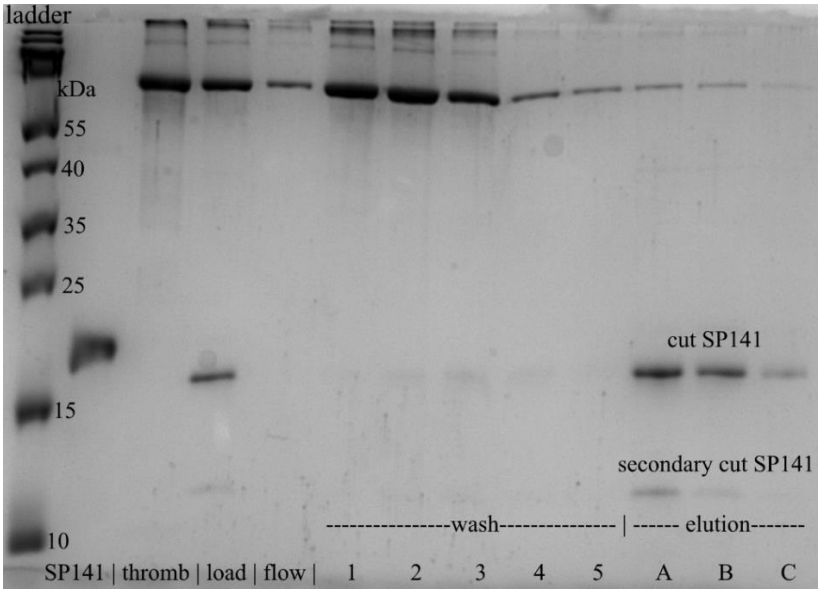

Figure 22 SDS-PAGE of thrombin cleavage followed by HisTag column purification; ladder (5µL, 1st lane), SP141uncut control (10µL, 2nd lane), thrombin control (10µL, 3rd lane); load on column (10µL, 4th lane), flowthrough (10µL, 5th lane), wash fractions 1-5 (10µL, 6th-10th lane); elution fractions A-C containing cut SP141thromb and 2ndary cut SP141thromb (10µL, 11th-13th lane); stained with Coomassie blue

4.3.4. Conjugation of SP141 to NTA-maleimide-linker

The conjugation of SP141 to the NTA-linker followed by SEC yielded the following SDS-PAGE in **Figure 23**. The observable splitting of the bands especially visible fraction A3 and A4 might be explained by the separation between the scaffolding proteins attached to the linker

and the ones not attached to the linker. Since the linker has a molecular weight of around 400 Da, it is reasonable that the weight-difference appears on the SDS-PAGE.

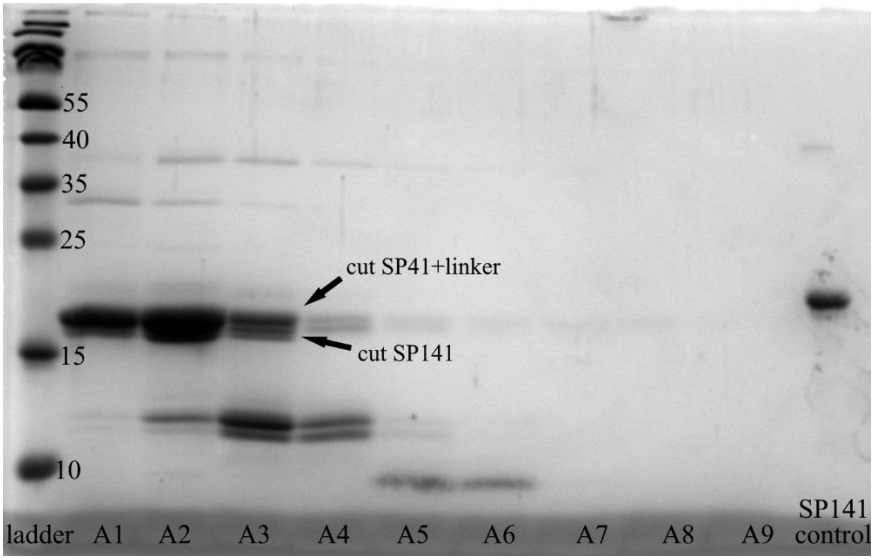

Figure 23 SDS-PAGE of SEC fractions after fusion with NTA-Maleimide linker; ladder (2µL, 1st lane); fractions A1-A9 (10µL; 2nd-10th lane); control SP141thromb (2µL; 11th lane); stained with Coomassie blue

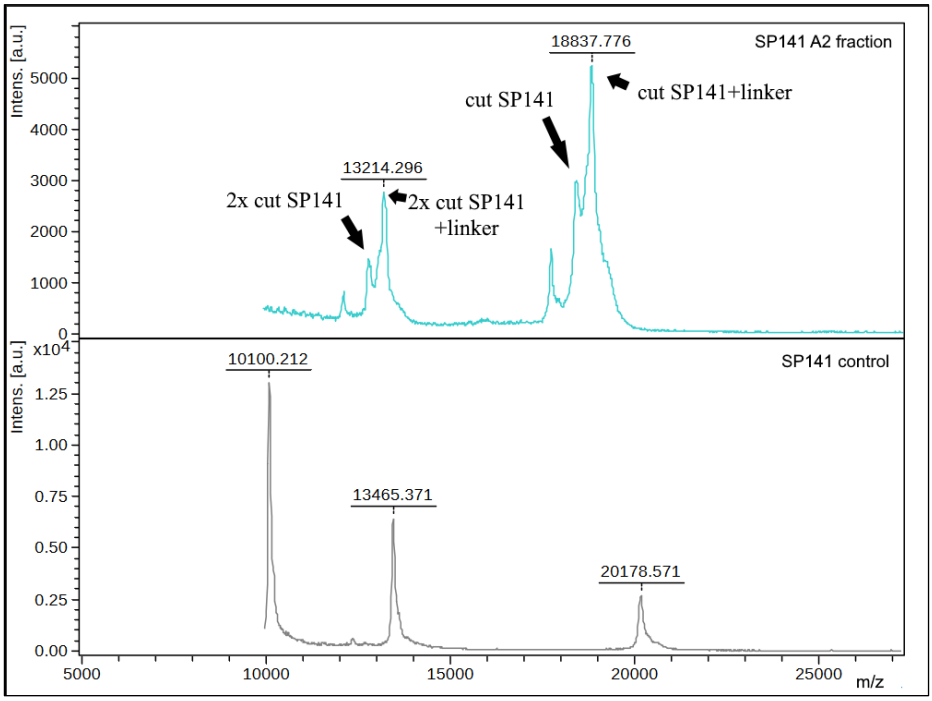

Figure 24 MS measurement of A2 fraction (top) and of a control SP141 (bottom)

That assumption is underlined further by MS measurements shown in **Figure 24**, where the main peak of the A2 fraction at 18.8 kDa corresponds to the sum of cut SP141 and NTA-maleimide (18.4 + 0.4 kDa). A slightly smaller peak at around 18.4 kDa can be observed as well and should correspond to the cut SP141 without linker. The same pattern can be

recognized for the secondary cut SP141 with a major peak at 13.2 kDa (2^{ndary} cut SP141+linker) and a smaller peak at around 12.8 kDa (2^{ndary} cut SP141). For the control, the peak at 20.2 kDa corresponds to the uncut SP141. The peak at 10.1 kDa seems to be a double charged SP141, and the peak at 13.5 kDa is unidentified. It is most likely an impurity.

A graphical explanation of the performed reaction can be seen in the following **Figure 25** inspired by the manual used for these reactions (Gruber, n.d.):

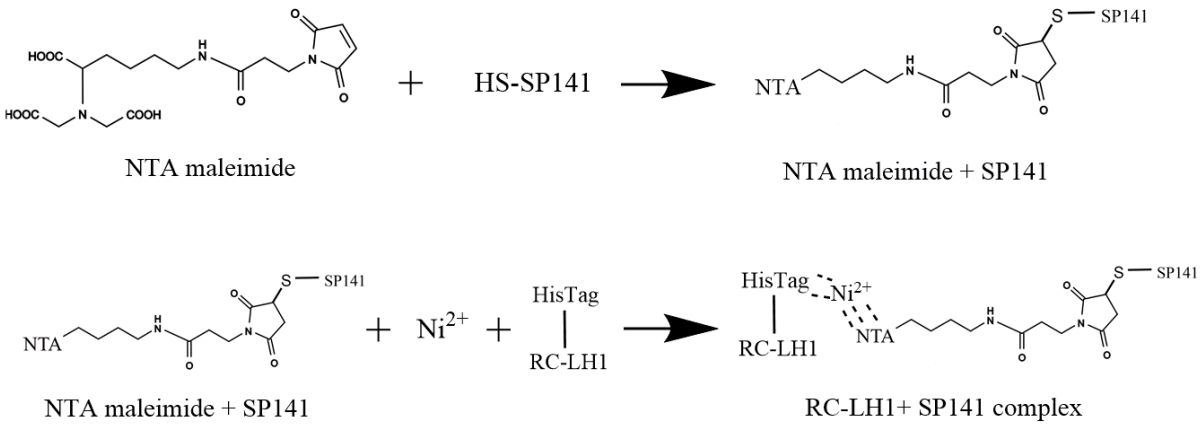

Figure 25 graphical representation of the performed reactions; 1st reaction: NTA-maleimide linker coupling to cyteine of SP141; 2nd reaction: NTA of linker-SP141 complex and HisTag of RC-LH1 conjugating nickel ions (Ni^{2+}) together, forming RC-LH1+SP141 complex

The NTA-Maleimide linker was fused to the N-terminal cysteine (-SH) of SP141thromb exposed by cleaving-off its HisTag. Thereby, the SP141 got equipped it with a functional NTA, being able to interact with a different HisTagged protein. Since the purified RC-LH1 contains a HisTag on its H-subunit, it can now interact with the functionalized SP141thromb, forming the RC-LH1+SP141 complex.

4.4. Encapsulation of RC-LH1 into capsids

Figure 26 shows an EM picture of the pure P22 capsids without RC-LH1 obtained from the purification in 3.2.5. They have a diameter of around 60 nm and generally show a dark inside, with a light shadow. Their shells appear lighter and mark a clear boundary to the background. On the other hand, the assembled capsids with potentially enclosed RC-LH1 can be observed in **Figure 27**. The RC-LH1 seems to appear as shiny rectangle and is clearly enclosed into the capsid. This picture features a lot more unfunctional capsids which could be explained by the

RC-LH1 interfering in capsid assembly. Unfunctional capsids can be recognized by the lack of dark in their interior. Their inside cannot be distinguished from the shell.

It can be stated that more data is needed to confirm the successful encapsulation of RC-LH1, it is however a first proof.

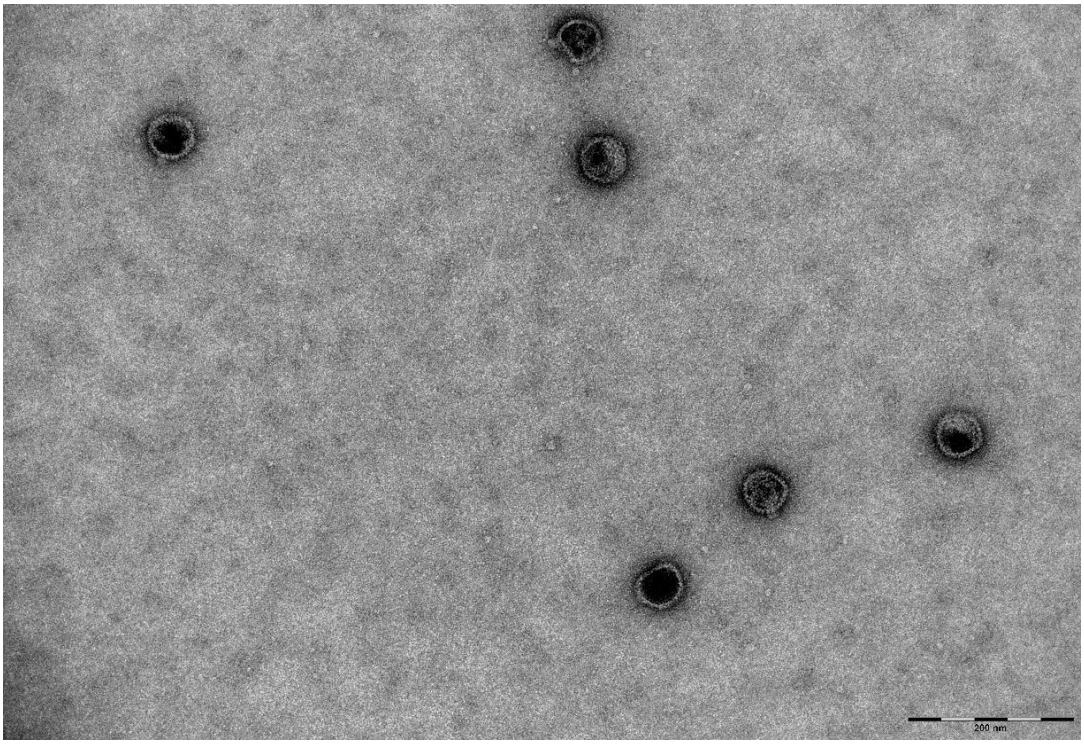

Figure 26 TEM picture of pure P22 capsids; 200 nm scale; negative staining

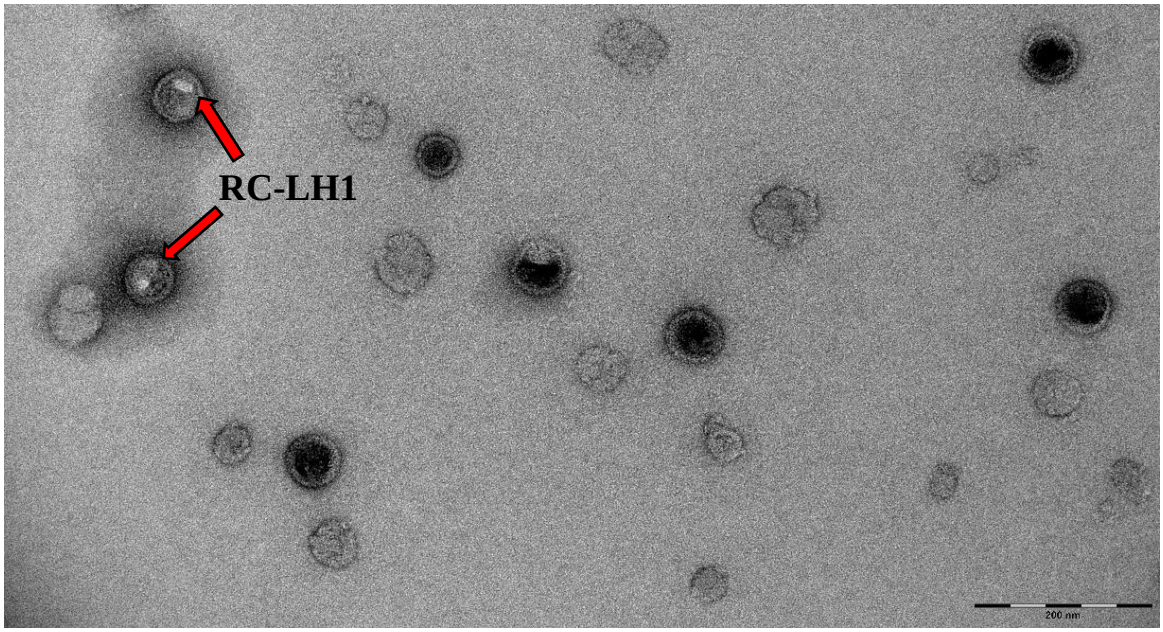

Figure 27 TEM picture of RC-LH1 (arrows) potentially encapsulated in P22 capsids; 200 nm scale; negative staining

5. Discussion

The final aim of this project was to encapsulate bacterial photosynthetic reaction centers into viral capsids. To achieve that, first the reaction center with light harvesting complex 1 of *Rhodobacter sphaeroides* had to be isolated and in parallel, also the viral capsids of bacteriophage P22. Second, the reaction center had to be coupled to the scaffolding protein of the capsid. This enabled the final assembly of all components to the viral capsids containing the reaction center with its light harvesting complex 1.

The purification steps were done using established protocols and to the HisTag on the reaction center and the scaffolding protein further facilitated it. Isolation of the reaction centers and the viral capsids yielded comparable results to those of Jun et al., 2014 and O'Neil et al., 2011. The obtained spectra of the reaction centers look like expected showing the highest absorbance in the infrared region. The obtained SDS-PAGE with its subunit assignment generally matches the reference (Jun et al., 2014). The EM pictures show nicely assembled capsids after purification resembling the results obtained by O'Neil et al., 2011 where the construct originates from.

In this case, the construct from O'Neil et al., 2011 enabling the incorporation of cargo-proteins into viral capsids could not be used in its original form, since only proteins expressible in *E. coli* such as GFP could be incorporated *in vivo*. The aim here is however to incorporate a membrane protein complex, namely a reaction center, not expressible in *E. coli*. This required two expression systems, *E. coli* and *R. sphaeroides* and final capsid assembly *in vitro*.

As in the original idea, it was tried to create a fusion product of the cargo-protein (reaction center here) and the scaffolding protein of the capsids, playing a major role in their assembly, thereby incorporating the cargo. This was tried by inserting the scaffolding protein gene behind the H-subunit gene (puhA) on the pIND4-RC1 plasmid encoding the photosynthetic operon of *R. sphaeroides*. With that the reaction center can be directly expressed with the scaffolding protein attached to its H-subunit sticking out of the membrane. Unfortunately, this method was tried over several different pathways unsuccessfully. These included special primer design and Gibson Assembly, but never achieved to obtain a functional plasmid construct. Problems could have been caused by secondary structures on the plasmid and the already heavily manipulated pIND4-plasmid with multiple restriction sites (Jun et al., 2018). It should be mentioned that this approach is still favorable over the alternative presented in the

following, since it includes less steps therefore being more efficient and could be tackled in further research.

The alternative plan included the attachment of an NTA maleimide linker to the cysteine of the scaffolding protein to functionalize it (Gruber, n.d.). This enabled its coupling to the reaction center due to interaction of the HisTag with the NTA. However, handling of the scaffolding protein was challenging because of the lacking thrombin cleavage site preventing the removal of its HisTag thereby exposing the cysteine. Therefore, the lacking thrombin site had to be fixed by genetic engineering, which turned out successful and enabled the HisTag removal by thrombin.

Successful thrombin cleavage and attachment of the linker was supported by SDS-PAGE and MS measurements. The final coupling to the reaction center, followed by the encapsulation of the reaction centers into the capsids was validated by TEM imaging. These images are however not final proof for the successful encapsulation and require further support, such as isolation of the given capsids and the reaction centers contained in them.

In the end, a great success was achieved with this study, since it is part of a bigger project aiming to create a photosynthetic nanoreactor observable in **Figure 28** (Lokstein & Tuma, n.d.). Therefore, in addition to the encapsulated reaction center providing the energy, the goal is to encapsulate further enzymes and proteins into the capsid utilizing this energy. These enzymes could then be chosen based on the application. They could be chosen in a way to fix carbon dioxide and produce methanol or produce compounds stereospecifically for the pharmaceutic industry.

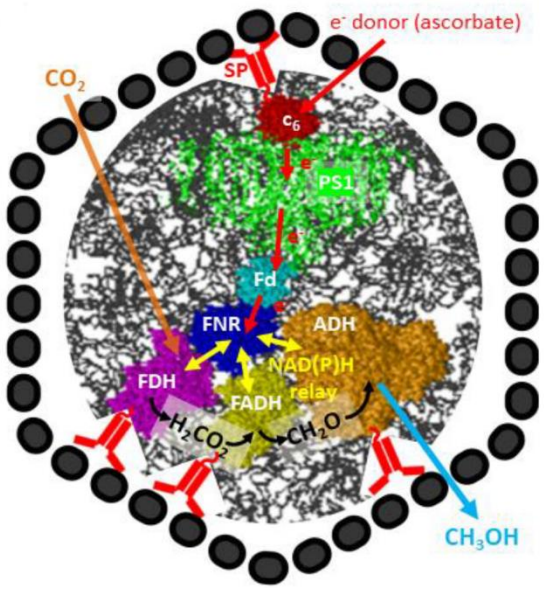

Figure 28 scheme of photosynthetic nanoreactor with P22 bacteriophage shell made of coat protein (black) containing: truncated scaffolding protein (SP, red) linked to different cargos; photosynthetic reaction center (PSI, green); ferredoxin (Fd); ferredoxin reductace (FNR); formate dehydrogenase (FDH); formaldehyde dehydrogenase (FADH); alcohol dehydrogenase (ADH). With capsid shell not to scale (Lokstein & Tuma, n.d.)

6. Conclusion

This project involved the expression and purification of reaction centers with light harvesting complex 1 from *Rhodobacter sphaeroides*, as well as of viral capsids from bacteriophage P22. The challenge was to encapsulate those reaction centers into the viral capsids being composed of coat protein forming the shell and scaffolding protein initiating assembly.

By attaching this scaffolding protein over an NTA maleimide linker to the HisTag of the reaction center, its enclosure into the capsids could be enabled. Therefore, the original HisTag containing scaffolding protein was genetically engineered by successful insertion of a thrombin cleavage site enabling the removal of the mentioned HisTag and attachment of the linker.

Successful assembly of capsids with encapsulated reaction centers was confirmed by transmission electron microscope pictures and shall be further supported by other methods. However, the whole process could be simplified by creation of a reaction center-scaffolding protein complex assembling in vitro, which could be tackled in further research.

In addition, these findings are the first step to create a functional nanoreactor on basis of P22 capsids powered by photosynthetic reaction centers such as the one of *Rhodobacter sphaeroides.* This would include encapsulation of additional enzymes and proteins along the reaction center utilizing the energy provided by the reaction center.

7. References

Adessi, A., & De Philippis, R. (2013). Purple Bacteria: Electron Acceptors and Donors. In *Encyclopedia of Biological Chemistry: Second Edition* (pp. 693–699). Elsevier Inc. https://doi.org/10.1016/B978-0-12-378630-2.00371-6

Aizawa, S.-I. (2014). Rhodobacter sphaeroides — A Resourceful Little Bug. In *The Flagellar World* (pp. 66–68). Elsevier. https://doi.org/10.1016/b978-0-12-417234-0.00021-9

Blankenship, R. E. (2014). *Molecular Mechanisms of Photosynthesis*. Wiley. https://books.google.at/books?id=4x_yAgAAQBAJ

Calendar, R. L. (Ed.). (2005). *The Bacteriophages* (2nd ed.). Oxford University Press.

Ciornii, D., Feifel, S. C., Hejazi, M., Kölsch, A., Lokstein, H., Zouni, A., & Lisdat, F. (2017). Construction of photobiocathodes using multi-walled carbon nanotubes and photosystem I. *Physica Status Solidi (A) Applications and Materials Science*, *214*(9). https://doi.org/10.1002/pssa.201700017

Donohue, T. J., & Kaplan, S. (1991). *[22] GENETICS OF PHOTOSYNTHETIC BACTERIA [22] Genetic Techniques in Rhodospirillaceae*.

DSMZ GmbH. (2010). *462. MINERAL MEDIUM (BRUNNER) WITH VITAMINS*. https://www.dsmz.de/microorganisms/medium/pdf/DSMZ_Medium462.pdf

Eaton-Rye, J. J., Tripathy, B. C., & Sharkey, T. D. (2012). *Photosynthesis: Plastid Biology, Energy Conversion and Carbon Assimilation*. Springer Netherlands. https://books.google.at/books?id=Q6JV3h2yqvUC

Friebe, V. M., & Frese, R. N. (2017). Photosynthetic reaction center-based biophotovoltaics. In *Current Opinion in Electrochemistry* (Vol. 5, Issue 1, pp. 126–134). Elsevier B.V. https://doi.org/10.1016/j.coelec.2017.08.001

Gruber, H. J. (n.d.). *Maleimide-PEG-TrisNTA linker coupling to the Cysteine of a protein*. http://www.jku.at/biophysics/content

Hanada, S. (2016). Anoxygenic photosynthesis —A photochemical reaction that does not contribute to oxygen reproduction—. *Microbes and Environments*, *31*(1), 1–3. https://doi.org/10.1264/jsme2.ME3101rh

Jaschke, P. R., Saer, R. G., Noll, S., & Beatty, J. T. (2011). *Modification of the Genome of Rhodobacter sphaeroides and Construction of Synthetic Operons* (pp. 519–538). https://doi.org/10.1016/b978-0-12-385075-1.00023-8

Jun, D., Dhupar, H. S., Mahmoudzadeh, A., Duong, F., Madden, J. D. W., & Beatty, J. T. (2018). In vivo assembly of a truncated H subunit mutant of the Rhodobacter sphaeroides photosynthetic reaction centre and direct electron transfer from the QA quinone to an electrode. *Photosynthesis Research*, *137*(2), 227–239. https://doi.org/10.1007/s11120-018-0493-0

Jun, D., Saer, R. G., Madden, J. D., & Beatty, J. T. (2014). Use of new strains of Rhodobacter sphaeroides and a modified simple culture medium to increase yield and facilitate purification of the reaction centre. *Photosynthesis Research*, *120*(1–2), 197–205. https://doi.org/10.1007/s11120-013-9866-6

Lokstein, H., & Tuma, R. (n.d.). *Light-driven energy conversion with biohybrid assemblies in nanocontainers*.

Lubner, C. E., Applegate, A. M., Knörzer, P., Ganago, A., Bryant, D. A., Happe, T., & Golbeck, J. H. (2011). *Solar hydrogen-producing bionanodevice outperforms natural photosynthesis*. https://doi.org/10.1073/pnas.1114660108/-/DCSupplemental

Lukashev, E. P., Knox, P. P., Gorokhov, V. V., Grishanova, N. P., Seifullina, N. K., Krikunova, M., Lokstein, H., & Paschenko, V. Z. (2016). Purple-bacterial photosynthetic reaction centers and quantum-dot hybrid-assemblies in lecithin liposomes and thin films. *Journal of Photochemistry and Photobiology B: Biology*, *164*, 73–82. https://doi.org/10.1016/j.jphotobiol.2016.09.009

Mackenzie, C., Eraso, J. M., Choudhary, M., Jung, H. R., Zeng, X., Bruscella, P., Puskás, Á., & Kaplan, S. (2007). Postgenomic adventures with Rhodobacter sphaeroides. In *Annual Review of Microbiology* (Vol. 61, pp. 283–307). https://doi.org/10.1146/annurev.micro.61.080706.093402

Madigan, M. T., Clark, D. P., Stahl, D., & Martinko, J. M. (2010). *Brock biology of microorganisms 13th edition*. Benjamin Cummings.

Nelson, N., & Ben-Shem, A. (2004). The complex architecture of oxygenic photosynthesis. In *Nature Reviews Molecular Cell Biology* (Vol. 5, Issue 12, pp. 971–982). Nature Publishing Group. https://doi.org/10.1038/nrm1525

Nelson, N., & Yocum, C. F. (2006). Structure and function of photosystems I and II. In *Annual Review of Plant Biology* (Vol. 57, pp. 521–565). https://doi.org/10.1146/annurev.arplant.57.032905.105350

O'Neil, A., Reichhardt, C., Johnson, B., Prevelige, P. E., & Douglas, T. (2011). Genetically programmed in vivo packaging of protein cargo and its controlled release from bacteriophage P22. *Angewandte Chemie - International Edition*, *50*(32), 7425–7428. https://doi.org/10.1002/anie.201102036

Orsi, E., Beekwilder, J., Eggink, G., Kengen, S. W. M., & Weusthuis, R. A. (2021). The transition of Rhodobacter sphaeroides into a microbial cell factory. In *Biotechnology and Bioengineering* (Vol. 118, Issue 2, pp. 531–541). John Wiley and Sons Inc. https://doi.org/10.1002/bit.27593

Potters, G., Van Goethem, D., & Schutte, F. (2010). Promising Biofuel Resources: Lignocellulose and Algae. *Nature Education*.

Ravi, S. K., Rawding, P., Elshahawy, A. M., Huang, K., Sun, W., Zhao, F., Wang, J., Jones, M. R., & Tan, S. C. (2019). Photosynthetic apparatus of Rhodobacter sphaeroides exhibits prolonged charge storage. *Nature Communications*, *10*(1). https://doi.org/10.1038/s41467-019-08817-7

Taiz, L., & Zeiger, E. (2010). *Plant Physiology*. Sinauer Associates. https://books.google.at/books?id=uPesjgEACAAJ

Tani, K., Kanno, R., Kikuchi, R., Kawamura, S., Nagashima, K. V. P., Hall, M., Takahashi, A., Yu, L. J., Kimura, Y., Madigan, M. T., Mizoguchi, A., Humbel, B. M., & Wang-Otomo, Z. Y. (2022). Asymmetric structure of the native Rhodobacter sphaeroides dimeric LH1–RC complex. *Nature Communications*, *13*(1). https://doi.org/10.1038/s41467-022-29453-8

ViralZone. (2015). *Lederbergvirus*. Https://Viralzone.Expasy.Org/519.

Yaghoubi, H., Li, Z., Jun, D., Saer, R., Slota, J. E., Beerbom, M., Schlaf, R., Madden, J. D., Beatty, J. T., & Takshi, A. (2012). The role of gold-adsorbed photosynthetic reaction centers and redox mediators in the charge transfer and photocurrent generation in a bio-

photoelectrochemical cell. *Journal of Physical Chemistry C*, *116*(47), 24868–24877. https://doi.org/10.1021/jp306798p